The Astronomical Journal, 123:1570–1602, March

A HIGH ANGULAR RESOLUTION MULTIPLICITY SURVEY OF THE OPEN CLUSTERS α PERSEI AND PRAESEPE

J. Patience[1] and A. M. Ghez
Division of Astronomy and Astrophysics, UCLA, Los Angeles, CA 90095-1562

and

I. N. Reid[2] and K. Matthews
Palomar Observatory, California Institute of Technology, 1201 East California Boulevard, Pasadena, CA 91125
Received 2001 June 19; accepted 2001 October 29

ABSTRACT

Two hundred forty-two members of the Praesepe and α Persei clusters have been surveyed with high angular resolution 2.2 μm speckle imaging on the 3 m Infrared Telescope Facility, the 5 m Hale, and the 10 m Keck telescopes, along with direct imaging using the near-infrared camera (NICMOS) aboard the *Hubble Space Telescope*. The observed stars range in spectral type from B ($\sim$5 $M_\odot$) to early M ($\sim$0.5 $M_\odot$), with the majority of the targets more massive than $\sim$0.8 $M_\odot$. The one quadruple and 39 binary systems detected encompass separations from 0$''$.053 to 7$''$.28; 28 of the systems are new detections, and there are nine candidate substellar companions. The results of the survey are used to test binary star formation and evolution scenarios and to investigate the effects of companion stars on X-ray emission and stellar rotation. The main results are as follows:

1. Over the projected separation range of 26 to 581 AU and magnitude differences of $\Delta K < 4.0$ (comparable to mass ratios $q = M_{\rm sec}/M_{\rm prim} > 0.25$), the companion-star fraction (CSF) for α Per is 0.09 $\pm$ 0.03, and that for Praesepe is 0.10 $\pm$ 0.03. This fraction is consistent with the field G dwarf value, implying that there is not a systematic decline in multiplicity with age at these separations on timescales of a few times 10^7 yr. The combination of previous spectroscopic work and the current cluster survey results in a cluster binary separation distribution that peaks at $4^{+1}_{-1.5}$ AU, a significantly smaller value than the peaks of both the field G dwarf and the nearby T Tauri distributions. If the field G dwarf distribution represents a superposition of distributions from the populations that contributed to the field, then the data imply that $\sim$30% of field binaries formed in dark clouds like the nearby T Tauri stars and the remaining $\sim$70% formed in denser regions.
2. An exploration of the binary star properties reveals a cluster CSF that increases with decreasing target mass, and a cluster mass ratio distribution that rises more sharply for higher mass stars but is independent of binary separation. These observational trends are consistent with several models of capture in small clusters and simulations of accretion following fragmentation in a cluster environment. Other types of capture and fragmentation are either inconsistent with these data or currently lack testable predictions.
3. Among the cluster A stars, there is a higher fraction of binaries in the subset with X-ray detections, consistent with the hypothesis that lower mass companions are the true source of X-ray emission.
4. Finally, in the younger cluster α Per, the rotational velocities for solar-type binaries with separations less than 60 AU are significantly higher than those of wider systems. This suggests that companions may critically affect the rotational evolution of young stars.

Key words: binaries: general — open clusters and associations: individual (α Persei, Praesepe)

1. INTRODUCTION

Extensive observations have established that binary stars are very common among field solar-type stars and are approximately twice as prevalent among T Tauri stars in the closest star-forming regions (Abt & Levy 1976; Duquennoy & Mayor 1991; Ghez, Neugebauer, & Matthews 1993; Ghez et al. 1997a; Leinert et al. 1993; Simon et al. 1995; Köhler & Leinert 1998). The large discrepancy in binary fractions between pre–main-sequence stars and main-sequence stars at separations of tens to hundreds of AU has provided the impetus for both theoretical studies (e.g., Kroupa 1995a, 1995b; Durisen & Sterzik 1994) and a number of high angular resolution imaging investigations of binary stars in nearby open clusters with ages intermediate between the pre–main-sequence stars ($\sim$2 Myr; Simon, Ghez, & Leinert 1993) and the solar neighborhood ($\sim$5 Gyr for the Duquennoy & Mayor 1991 sample). An adaptive optics survey of the Pleiades ($\sim$125 Myr; Stauffer, Schultz, & Kirkpatrick 1998) measured a binary fraction comparable to that of the field over the separation range 11 to 792 AU (Bouvier, Rigaut, & Nadeau 1997). In contrast, a speckle imaging survey of the older Hyades ($\sim$660 Myr; Torres, Stefanik, & Latham 1997), covering the 5–50 AU separation range, measured a multiplicity intermediate between the T Tauri and the field stars (Patience et al. 1998). In this paper, the multiplicity of α Per (90 Myr; Stauffer et al. 1999) and Praesepe ($\sim$660 Myr; Mermilliod 1981) is investigated using speckle imaging with large ground-based telescopes and direct imaging with the *Hubble Space Telescope* (*HST*). The

[1] Current address: Institute of Geophysics and Planetary Physics, L-413, Lawrence Livermore National Laboratory, 7000 East Avenue, Livermore, CA 94550; patience@igpp.ucllnl.org.
[2] Current address: Space Telescope Science Institute, 3700 San Martin Drive, Baltimore, MD 21218.

first aspect of this project addresses the disparity in binary fractions by measuring the evolution of the binary star fraction over the critical separation range of tens to hundreds of AU.

The database of binary star characteristics resolved by large multiplicity surveys can also be used to observationally test several binary star formation scenarios. Binary star formation mechanisms fall into two broad categories, capture and fragmentation (see, e.g., the review in Clarke 1996a). Although capture in large clusters does not occur frequently enough to produce a significant fraction of binaries (Aarseth & Hills 1972), capture in small-N clusters with or without the effects of circumstellar disks has been modeled as a viable formation mechanism (McDonald & Clarke 1993, 1995; Sterzik & Durisen 1998). Different modes of fragmentation have also been proposed—fragmentation of the protostellar cloud core (see, e.g., Clarke 1996a) or of the protostellar disk (e.g., Bonnell & Bate 1994); other simulations follow the accretion of material after fragmentation (Bonnell & Bate 1997; Bate 2000, 2001). Many formation theories have distinct predictions for the resulting binary star properties, such as how the companion-star fraction and mass ratio distribution depend upon mass. In order to investigate the mass dependence of these properties, the stars surveyed for this work cover a range of masses, from the massive B stars to the subsolar-mass late K and early M stars ($\sim$5 to $\sim$0.5 $M_{\odot}$).

Another topic that can be addressed with multiplicity surveys is the effect, both active and passive, of a companion on the primary. Of particular interest for this study is the possible active role of binary companions in the rotational history of solar-type stars. Although most solar-type stars have low rotational velocities ($\sim$15 km s^{-1}) with a limited spread in values ($\sim$6–70 km s^{-1}) during the pre–main-sequence stage (see, e.g., Bertout 1989), by the age of the α Per cluster, 90 Myr, these stars exhibit a range of rotational velocities of more than 200 km s^{-1} (Stauffer et al. 1985; Prosser 1992). While the subsequent spin-down due to mass loss in a magnetized wind is well understood (Schatzman 1962), the mechanism that makes some stars rapid rotators, while most remain slow rotators at the age of α Per, is not known; two opposing ideas, however, involve binary stars. Both scenarios are predicated upon the assumption that stellar rotation is regulated by a star-disk interaction (Königl 1991; Armitage & Clarke 1996) in which the stellar magnetic field is linked to the slowly rotating outer disk. In the disk-braking scenario, the stellar rotation rate is critically dependent upon the circumstellar disk lifetime, with the rapid rotators associated with short-lived disks. One model suggests that binary stars completely disrupt the circumstellar disks, creating rapid rotators (Bouvier et al. 1997), while an alternate theory suggests that except for tidally locked systems, binary stars should be slow rotators. In the second model, binary stars truncate rather than obliterate disks, leaving a remnant ring of material that actually survives longer and brakes the star over a longer period of time (Armitage & Clarke 1996). Recent observations of rotation periods among Trapezium stars have questioned the idea of disk-regulated rotation (Stassun et al. 1999), but this Orion study focused on lower mass stars than those observed in α Per, and mass may be an important factor in rotation rates (Herbst et al. 2000). Angular momentum evolution varies with mass, and therefore this part of the investigation is limited to the solar-type stars. With the maximum range of rotational velocities, α Per is the ideal cluster to investigate this possible role of companions.

A potential passive effect of companions relates to X-ray detections; late-type companion stars may be an important factor in explaining the X-ray detections from late B and A-type stars. B6–A5 stars lack both the strong winds of higher mass stars and the dynamo of lower mass stars believed to generate X-rays along the rest of the main sequence (cf. Pallavicini 1989). While shearing motions in the coronae of late B to A stars may represent a mechanism to generate X-rays (Tout & Pringle 1995), unresolved companions may be the true source of the observed X-rays and provide a simpler explanation. Multiplicity surveys test this hypothesis, as binaries discovered by spectroscopy or by the current high-resolution imaging survey have separations smaller than typical $\sim$10″ *ROSAT* detection error boxes.

In this paper, the results of high angular resolution multiplicity surveys of α Per and Praesepe are reported and are used to investigate the formation and evolution of binaries, as well as the role of companions in stellar rotation and X-ray emission. The data were obtained using speckle imaging on large ground-based telescopes and direct imaging with *HST* for an additional set of fainter stars. The samples are defined in § 2, and the observations and data analysis are described in § 3. The results and a description of the sensitivity are reported in § 4, which also details the sensitivities of several comparison surveys. In the discussion, §§ 5–7, the evolution of both the binary fraction and the binary separation distribution are investigated, the companion-star fraction and the mass ratio distribution are compared with theoretical models, and the connection between binarity and X-ray emission and stellar rotation is explored. The main conclusions are summarized in § 8.

2. THE SAMPLE

The two clusters selected for this study, α Per and Praesepe, are ideal samples for multiplicity surveys, as these clusters share two critical properties—distances comparable to the nearby star-forming regions and ages intermediate between T Tauri stars and field stars. The younger cluster, α Per, has an age of 50 to 90 Myr (Prosser 1992; Stauffer et al. 1999), with the most recent age assessment based on the lithium depletion boundary giving the larger value; the more recent value is used in this study. The distance to α Per is 176 ± 5 pc (Pinsonneault et al. 1998). The older cluster, Praesepe, has an age of $\sim$660 Myr (Mermilliod 1981) and a distance of 171 ± 4 pc (Pinsonneault et al. 1998). The spatial extent of the clusters, 10 to 15 pc in diameter, introduces an additional uncertainty in the distances to individual members.

The stars observed for this survey were drawn from cluster membership studies with the additional criteria of $K \lesssim 10$ mag for the speckle data and 10 mag $< K <$ 12.3 mag for the α Per *HST* data. The range of masses for the α Per stars is $\sim$5 to $\sim$0.5 $M_{\odot}$. K_s magnitudes are available for almost the entire sample from the 2MASS catalog; Appendix B describes the conversion from K_s to K magnitudes. Only three giants in Praesepe exceed the 2MASS magnitude limit; however, these stars are not included in the analysis of binary properties. For the 25 α Per and six Praesepe main-sequence stars not covered in the current 2MASS data release, the K magnitudes were estimated from an empirical V magnitude–to–K magnitude relation based on a fit to the

observed stars; a separate fit was made for each cluster. Again, the details of the V-to-K relation are given in Appendix B. Tables 1 and 2 list the observed samples of α Per and Praesepe. Each table gives the name, J2000 coordinates, V magnitude, $B-V$ color, spectral type, 2MASS K magnitude, and X-ray flux or upper limit; for α Per, the measured $v \sin i$ is also listed in Table 1.

The stars in the α Per speckle sample have spectral types from B to G, range in K magnitude from 5.1 to 10.5, and account for 109 of the 112 brightest (based on V magnitudes) stars with definite membership. An additional 33 fainter stars with K magnitudes between 10.0 and 12.3 and a large range of rotational velocities were observed with *HST*. In total, the α Per sample comprises 142 stars. Because of the lower Galactic latitude (-7°) of α Per, a combination of proper motions, radial velocities, and indications of stellar activity (Hα, Li features) is required to assess the membership of each star in the younger cluster; results from studies of the brighter stars (Heckmann, Dieckvoss, & Kox 1956) and the fainter stars (Stauffer et al. 1985; Prosser 1992) are compiled in Prosser (1992).

The Praesepe speckle sample includes most of the brightest stars in the cluster, with spectral types from A to G; the 100 observed stars represent more than half of the Klein Wassink (1927) membership list, which is based upon photometry and proper motion. Excluding the giants, the range of K magnitudes is 5.9 to 9.2, corresponding to masses for the Praesepe main-sequence stars of $\sim$2.4 to $\sim$1.0 $M_\odot$. More recent spectroscopic observations of Praesepe stars have revealed a few Klein Wassink stars as nonmembers (Mermilliod & Mayor 1999), and two of these nonmember stars are part of the speckle sample—KW 258 and KW 553. The results for these two stars are reported, but they are not included in the analysis.

3. OBSERVATIONS AND DATA ANALYSIS

3.1. *Ground-based Speckle Imaging and Shift-and-Add*

For this study, speckle imaging data were obtained through the K-band ($\lambda_0 = 2.2$ μm, $\Delta\lambda = 0.4$ μm) filter with three different cameras: the facility near-infrared camera on the 5 m Hale Telescope at Palomar Observatory, NSFCAM (Rayner et al. 1993; Shure et al. 1994) on the 3 m NASA Infrared Telescope Facility (IRTF), and NIRC (Matthews & Soifer 1994; Matthews et al. 1996) on the 10 m Keck I Telescope. With plate scales of $0\farcs0326$ pixel^{-1} for Palomar, $0\farcs0532$ pixel^{-1} for NSFCAM, and $0\farcs0206$ pixel^{-1} for NIRC, each camera allows for diffraction-limited imaging at 2.2 μm. The diffraction limit, λ/D, ranges from $0\farcs045$ to $0\farcs15$ for these observations. All the cameras include 256×256 arrays; however, only subarrays were recorded at Palomar and the IRTF. Because of demands on the available disk space, the Palomar data are limited to a 64×64 subarray, or a $2\farcs14 \times 2\farcs14$ field of view, and the IRTF data are restricted to a 128×128 subarray, resulting in a wider $6\farcs80 \times 6\farcs80$ field of view.

The observing program was designed to obtain a sample as large as possible, but also to ensure that the survey data covered a large angular separation range. The survey was initiated in 1995 at Palomar and completed in 1999 at the IRTF; a small sample was also observed in 1999 at Keck to begin to probe smaller separations. Speckle analysis is particularly effective for resolving binaries with separations close to the diffraction limit, while shift-and-add processing is most effective for detecting companions outside the seeing halo (radius $\sim 0\farcs5$) of the target star. Table 3 summarizes the number and type of observations made for the sample. The entire ground-based sample was observed with one of the three cameras for full speckle analysis. Almost all the targets observed from the ground were also analyzed with the shift-and-add technique.

The speckle observing procedure is the same for each camera and involves recording a total of 3000 to 4000 exposures (fewer for Keck) of $\sim$0.1 s in stacks of $\sim$500 images. By alternating between observations of the target star and a nearby reference point source, atmospheric effects are measured and removed through analysis developed by Labeyrie (1970) and Lohmann, Weigelt, & Wirnitzer (1983). Details of the data analysis are given in Ghez et al. (1993) and Patience et al. (1998). The results of the speckle processing of binary stars determines the magnitude difference ΔK between primary and secondary, the projected separation, and the position angle, while the parameters measured for single stars are detection limits for unseen companions calculated for several separations.

In addition to speckle analysis, nearly all the stars in each cluster were also processed with the shift-and-add technique (Bates & Cady 1980; Christou 1991). The speckle data collected with the wider field NSFCAM and NIRC cameras were all reanalyzed with this method to search for wider companions. In order to have uniform coverage at the widest separations, all but nine α Per and 11 Praesepe stars observed at Palomar were reobserved at the IRTF for shift-and-add analysis; the shift-and-add data sets require fewer frames and are more efficient to obtain. The shift-and-add analysis provides the same parameters for binary and single stars as the speckle procedure (see Ghez et al. 1998 for details).

3.2. *Direct Imaging with the Hubble Space Telescope*

HST observations with the onboard near-infrared camera NICMOS (Thompson et al. 1998) were taken of 33 members of α Per fainter than the speckle limiting magnitude ($K \sim 10$). Using the highest resolution camera of NICMOS—NIC1—which has a pixel scale of $0\farcs043$ pixel^{-1} (Thompson et al. 1998), images were recorded through the F140W filter ($\lambda_0 = 1.3$ μm, $\Delta\lambda = 1.0$ μm) in order to maximize sensitivity to companion stars. With the shorter wavelength F140W filter, the diffraction-limited resolution (λ/D) for *HST* is $0\farcs11$, comparable to the ground-based K-band speckle observations that constitute the majority of the survey data set. To minimize the effects of bad pixels, two offset images were obtained for each target. The data were taken in the MULTIACCUM mode, which performs a series of nondestructive readouts designed to increase the dynamic range of the observations. The integration time was at least 2 minutes for each star and as high as 10 minutes for some stars, depending upon how efficiently groups of stars could be packed into a single *HST* orbit. As with the speckle and shift-and-add analysis, the *HST* data reduction results determine the magnitude difference—in this case ΔF140W—between primary and secondary, the projected separation, and the position angle for binary stars and the ΔF140W detection limits for unseen companions for the single stars. The IRAF PHOT package was used to measure the magnitudes and positions of the binaries and the detec-

TABLE 1

α PERSEI SAMPLE

Object	BD	HD	R.A.[a] (J2000)	Decl.[a] (J2000)	V[a]	$B-V$[a]	Sp.[a]	K	log L_X[b]	log L_X[c]	$v \sin i$ (km s^{-1})	Tel.[d]
HD 18537	+51°665	...	3 00 52.0	52 21 07	5.00	−0.04	B7 V	5.468	...	...	220	I
HD 18538	+51°665B	...	3 00 53.3	52 21 08	6.74	0	B9 V	6.691	...	...	...	I
HE 12.....	+48°851	...	3 07 50.3	49 06 30	10.09	0.51	F6 V	8.797	...	...	49	P, I
HE 56.....	...	...	3 09 51.9	48 28 16	10.84	0.81	G3 V	9.007	...	...	<10	P, I
HE 93.....	...	...	3 10 41.6	50 31 32	11.09	0.7	G4	9.275	...	...	12	I
HE 92.....	...	...	3 10 44.2	50 20 47	11.06	0.65	...	9.788	...	...	27	I
HE 94.....	...	...	3 11 16.6	48 10 37	10.42	0.64	F9 V	8.728	...	...	...	K
HE 104.....	+47°776	19655	3 11 40.9	48 03 16	8.60	0.34	F2 Vn	7.778	...	...	> 200	P, I
HE 135.....	+49°868	...	3 11 49.8	50 22 48	9.71	0.49	F5 V	8.556	...	...	16	I
HE 143.....	+49°870	...	3 12 02.9	50 23 32	10.47	0.71	F8 IV–V	8.738	...	...	<10	P, I
HE 151.....	+47°780	19767	3 12 42.5	47 50 20	8.97	0.32	F0 Vn	8.156	...	...	140	I
HE 167.....	+48°862	19805	3 13 05.1	49 00 35	7.94	0.12	B9.5 V	7.679	...	...	<20	P, I
HE 212.....	+49°876	19893	3 13 50.2	49 34 09	7.15	0.04	B9 V	7.070	...	...	280	P, I
HE 220.....	+48°865	19954	3 14 16.5	48 34 41	9.14	0.33	A3	8.328	...	...	85	I
HE 270.....	+48°871	...	3 15 23.4	49 26 26	10.11	0.51	F7 V	8.861	...	...	33	I
HE 299.....	...	...	3 15 58.6	50 24 19	11.19	0.64	F7	9.582	...	...	17	I
HE 285.....	+47°792	20135	3 16 01.8	48 01 41	8.09	0.21	A0p	7.400	...	...	35	P, I
HE 314.....	+50°728	20122	3 16 13.4	51 25 45	9.25	0.43	F2 V	8.164	...	...	110	I
HE 309.....	...	...	3 16 23.0	49 37 34	9.96	0.49	F5 V	8.805	...	...	65	K
HE 334.....	+49°892	...	3 16 48.9	51 13 07	7.19	0.03	B9	7.028	...	...	19	P, I
HE 333.....	+50°731	20191	3 16 59.2	49 55 37	10.37	0.55	F7 V	9.038	...	...	230	P, I
HE 338.....	+48°876	...	3 17 20.1	49 30 09	9.93	0.56	F7 V	8.621	...	...	56	P, I
HE 350.....	...	...	3 17 36.7	48 50 09	11.13	0.71	G3	9.268	...	29.81	47	P, I
AP 121	...	...	3 17 42.1	49 01 48	11.89	0.79	G5	9.865	<29.69	...	<10	I
HE 361.....	+49°896	...	3 18 01.6	49 38 40	9.68	0.44	F4 V	8.614	...	...	30	I
HE 365.....	+49°897	...	3 18 05.0	49 54 22	9.90	0.5	F6 V	8.716	...	...	108	I
HE 373.....	...	...	3 18 27.3	47 21 17	11.50	0.77	G3	9.421	...	...	140	I
HE 383.....	+49°899	20365	3 18 37.5	50 13 21	5.15	−0.06	B3 V	5.312	...	...	145	P, I
HE 386.....	+49°900	20391	3 18 44.6	49 46 13	7.93	0.12	A2 V	7.663	...	...	260	I
AP 90	...	...	3 18 49.9	49 43 53	11.17	0.67	F9	9.523	...	...	<10	I
AP 92	...	...	3 19 02.0	49 33 38	15.68	1.5	...	11.234	<29.82	...	90	H
AP 93	...	...	3 19 02.3	48 10 57	11.99	0.93	...	9.433	...	30.18	75	K
HE 401.....	+49°902	20418	3 19 07.5	50 05 43	5.04	−0.08	B5 V	5.203	<29.63	...	320	I
HE 407.....	...	...	3 19 19.4	50 44 49	11.18	0.64	A2	9.499	...	...	28	P, I
HE 421.....	+48°885	20475	3 19 41.5	48 54 50	9.23	0.45	F2 V	8.010	30.1	30.02	90	I
AP 125	...	...	3 19 45.6	50 08 36	12.16	...	...	10.100	<29.48	...	48	H
HE 423.....	+48°886	20487	3 19 47.1	48 37 42	7.64	0.07	A0 Vn	7.481	<29.36	<29.28	280	I
AP 95	...	...	3 19 57.3	49 52 07	12.28	0.88	...	9.934	29.88	<29.91	140	H
AP 127	...	...	3 20 01.4	46 53 08	12.57	1.12	...	9.894	...	...	80	H
AP 97	...	...	3 20 41.4	48 24 36	12.08	0.87	G6.5	9.909	<29.53	29.52	<10	I
AP 98	...	...	3 21 06.1	48 26 11	12.80	1	G9	10.325	<29.39	29.11	<10	H
AP 100	...	...	3 21 15.6	48 35 06	12.80	1.13	...	9.599	29.87	29.72	205	H
AP 102	...	...	3 21 19.9	48 45 27	11.96	0.8	...	9.849	29.68	29.7	11	I
AP 101	...	...	3 21 22.1	49 57 03	13.89	1.25	K6	10.436	29.37	<29.99	<10	H
HE 481.....	+47°808	...	3 21 30.1	48 29 39	9.18	0.36	F1 IVn	8.219	<29.27	<28.85	180	I
HE 490.....	+48°892	...	3 21 40.1	49 07 13	9.59	0.43	F3 IV–V	8.489	28.85	<29.11	15	I
AP 104	...	...	3 22 04.8	48 49 36	12.06	0.78	G3.5	10.193	<28.95	<28.90	<10	I
AP 139	...	...	3 22 06.8	47 34 08	12.00	...	...	9.782[e]	...	29.86	> 200	K
HE 520.....	...	...	3 22 21.8	49 08 29	11.69	0.79	G3	9.651	30.38	30.29	87	I
AP 106	...	...	3 22 40.6	49 40 42	12.94	1.01	...	10.460	29.61	29.52	<10	H
HE 557.....	+48°899	20809	3 23 13.0	49 12 49	5.26	−0.08	B5 V	5.558	<28.96	<28.90	250	P
AP 108	...	...	3 23 36.3	48 58 53	12.92	1.03	...	10.340	29.8	29.85	14	H
AP 6	...	...	3 23 42.4	49 10 32	15.53	1.56	...	11.327	<28.95	...	<15	...
HE 575.....	+51°728	20842	3 23 43.0	51 46 15	7.85	0.1	A0 V	7.554	...	...	85	P, I
HE 581.....	+48°903	20863	3 23 47.2	48 36 17	6.99	0.01	B9 V	6.902	30.49	30.35	200	P
HE 588.....	+49°914	...	3 23 54.9	50 18 25	10.01	0.54	F5 V	8.485	29.8	...	120	P, I
AP 14	...	...	3 24 19.8	48 47 20	11.94	0.83	G4	9.971	29.73	29.62	<10	I
HE 609.....	+49°918	...	3 24 24.9	50 19 35	9.23	0.42	F0 V	7.996	30.07	...	175	I
AP 15	...	...	3 24 25.0	48 48 22	14.12	1.29	...	10.744	29.86	29.58	52	H
HE 612.....	+48°906	20931	3 24 29.8	49 08 25	7.87	0.09	A1 V	7.712	<28.96	<29.04	85	P, I
AP 17	...	...	3 24 32.1	49 18 29	15.27	1.55	...	10.947	29.76	29.3	> 60	H
HE 621.....	+47°816	...	3 24 46.9	48 24 43	9.86	0.49	F4 V	8.724	<29.30	<28.95	28	I
AP 149	...	...	3 24 48.3	48 53 21	11.71	0.82	...	9.502	30.33	30.23	117	H
AP 19	...	...	3 24 49.6	48 52 20	11.62	0.79	...	9.624	30.39	30.44	61	H

TABLE 1—*Continued*

Object	BD	HD	R.A.[a] (J2000)	Decl.[a] (J2000)	V[a]	$B-V$[a]	Sp.[a]	K	log L_X[b]	log L_X[c]	$v \sin i$ (km s^{-1})	Tel.[d]
HE 625.....	+47°817	20961	3 24 51.9	47 54 56	7.63	0.11	B9.5 V	7.338	...	<29.04	25	P, I
AP 20.....	...	...	3 24 52.4	49 04 16	15.66	1.55	...	10.906	29.7	29.11	70	H
HE 632.....	+46°745	...	3 24 54.9	47 24 55	9.73	0.46	F4 V	8.676[e]	...	<29.63	160	I
AP 110.....	...	...	3 24 55.7	50 01 52	12.27	0.92	G8	10.058	29.48	<30.00	<10	K
AP 21.....	...	...	3 25 01.2	49 02 06	15.56	1.6	...	11.103	29.58	29.2	25	H
HE 639.....	+48°907	20986	3 25 09.8	49 15 07	8.15	0.12	A3 Vn	7.882	<29.13	<28.9	210	P, I
AP 25.....	...	...	3 25 16.1	48 22 24	12.25	0.88	...	10.008	29.73	30.12	12	H
HE 651.....	+48°909	21005	3 25 20.6	49 18 59	8.42	0.19	A5 Vn	8.029	<29.16	<28.95	250	I
AP 112.....	...	...	3 25 31.8	48 30 09	13.72	1.13	...	10.610	29.57	29.9	13	H
HE 665.....	+46°748	21046	3 25 37.5	47 01 16	8.64	0.29	A7 V	8.050[e]	...	...	70	P
AP 28.....	...	...	3 25 53.8	48 31 09	13.09	1.05	...	10.432	29.59	29.8	12	H
HE 675.....	+48°913	21071	3 25 57.2	49 07 16	6.06	−0.08	B7 V	6.315	<29.20	<28.90	70	P, I
HE 684.....	...	...	3 26 04.1	48 48 09	10.59	0.57	F9 V	9.201	30.2	30.12	71	P, I
AP 37.....	...	...	3 26 16.3	48 50 29	12.61	0.96	...	10.295	29.91	29.96	29	H
HE 696.....	...	...	3 26 19.2	49 13 34	11.61	0.76	G3	9.727	29.81	29.81	10	I
HE 699.....	...	...	3 26 22.1	49 25 39	11.27	0.71	G1 V	9.416	30.18	30.36	90	I
AP 156.....	...	...	3 26 22.6	47 16 10	11.89	...	G6	9.733[e]	...	...	<10	I
AP 41.....	...	...	3 26 25.3	48 20 07	12.03	0.85	G5	9.894	<29.56	29.45	10	H
AP 43.....	...	...	3 26 27.5	49 02 13	12.84	0.97	...	10.129	30.16	29.99	72	H
AP 158.....	...	...	3 26 03.7	50 13 55	11.93	0.85	...	9.736	29.4	...	13	I
HE 715.....	...	...	3 26 40.5	48 46 38	9.75	0.48	F4 V	8.687[e]	30.03	29.15	110	I
HE 709.....	...	...	3 26 43.8	49 54 35	10.95	0.68	G0 V	9.299[e]	30.46	30.26	59	P, I
HE 727.....	...	...	3 26 49.9	48 47 33	10.32	0.56	F7 V	8.987[e]	30.18	30.09	70	P, I
HE 735.....	+47°828	21185	3 27 05.1	48 12 21	6.83	−0.02	BVn..	6.811[e]	...	<28.85	345	P, I
AP 56.....	...	...	3 27 23.3	48 22 25	13.00	1	...	10.305	<29.64	29.72	110	H
HE 750.....	...	...	3 27 37.6	48 59 30	10.59	0.59	F9 V	9.206	<29.55	29.18	26	P, I
AP 60.....	...	...	3 27 38.5	48 25 00	15.74	1.7	...	10.865	<29.77	29.4	105	H
AP 63.....	...	...	3 27 50.9	49 12 11	12.29	0.92	...	9.919	<29.56	29.81	...	K
HE 767.....	...	...	3 27 54.9	49 45 38	10.69	0.62	F9 V	9.204	<29.36	<29.38	10	P, I
HE 775.....	+47°831	21279	3 27 55.6	47 44 10	7.26	0.05	B8.5 V	7.133[e]	...	<29.26	200	I
HE 774.....	+48°920	21278	3 28 02.9	49 03 48	4.97	−0.09	B5 V	5.243	<29.57	<28.90	65	I
HE 780.....	...	...	3 28 18.4	49 57 11	8.09	0.17	A1 Vn	7.547	30.12	29.74	230	K
AP 70.....	...	...	3 28 18.6	48 39 49	12.83	1	K0	10.274	<29.66	29.68	<10	H
AP 72.....	...	...	3 28 22.5	49 14 30	12.78	0.99	K0	10.443	<29.63	28.7	<10	H
HE 799.....	+48°923	...	3 28 31.4	48 56 28	9.66	0.45	F4 V	8.636	<29.67	29	20	I
AP 75.....	...	...	3 28 47.3	49 16 28	13.82	1.27	...	10.296	<29.56	29.43	11	H
AP 117.....	...	...	3 28 48.3	49 11 54	13.05	0.95	...	10.367	<29.83	29.89	83	H
HE 810.....	+49°944	21362	3 28 52.2	49 50 55	5.58	−0.04	B6 Vn	5.687	<29.36	<29.28	385	P, I
HE 817.....	+48°927	21375	3 28 53.5	49 04 14	7.46	0.11	A1 V	7.153	<29.78	29.45	270	P, I
HE 828.....	...	...	3 28 59.5	48 14 10	11.62	0.71	F8	9.748	...	29.2	10	I
HE 831.....	+47°835	21398	3 29 07.5	48 18 12	7.36	0.01	B9 V	7.354	...	<28.85	135	P, I
HE 833.....	...	...	3 29 08.1	48 10 52	10.05	0.42	F6 V	8.806	...	<29.18	30	I
AP 173.....	...	...	3 29 14.1	49 41 18	12.26	...	K3.2	9.784	...	<29.38	<10	K
HE 835.....	+49°945	21428	3 29 21.9	49 30 33	4.66	−0.1	B3 V	4.881	30.15	30.05	190	I
HE 841.....	...	...	3 29 24.8	48 57 46	10.29	0.54	F7 V	8.944	...	30.02	65	P, I
HE 848.....	...	...	3 29 26.1	48 12 13	10.00	0.6	...	8.537	...	29.53	<20	P, I
AP 78.....	...	...	3 29 26.5	49 20 36	13.06	1.02	...	10.475	<29.56	29.72	13	H
HE 862.....	+48°930	21480	3 29 46.9	49 09 15	8.52	0.31	A7 V	7.809	<29.56	<28.85	50	P, I
HE 868.....	+48°933	21479	3 29 51.7	49 12 50	7.28	0.09	A1 IVn	7.034	<29.56	<28.78	180	P, I
HE 885.....	+48°934	21527	3 30 19.1	48 29 59	8.79	0.28	A7 IV	8.192	...	29.2	80	I
AP 86.....	...	...	3 30 22.4	48 24 42	14.31	1.32	...	10.780	...	29.3	140	H
HE 906.....	+47°842	21553	3 30 33.8	47 37 43	8.78	0.28	A6 Vn	8.135[e]	...	<29.15	150	I
HE 904.....	+47°844	21551	3 30 36.8	48 06 14	5.82	−0.04	B8 V	5.936	...	<28.90	380	I
HE 917.....	...	...	3 30 47.5	47 53 23	10.93	0.66	F4	9.256	...	30.21	40	P, I
HE 921.....	+49°953	21600	3 31 14.5	49 42 24	8.59	0.2	A6 Vn	8.158	<28.99	<29.30	200	I
HE 935.....	...	...	3 31 28.8	48 59 30	10.05	0.62	...	8.847[e]	...	30.62	78	P, I
HE 931.....	+49°954	21619	3 31 30.1	49 54 09	8.75	0.26	A6 V	8.180	<28.90	<29.76	90	I
HE 955.....	+47°380	21641	3 31 32.9	47 51 46	6.75	−0.02	B8.5 V	6.796	...	<29.08	215	P, I
HE 944.....	+49°957	...	3 31 44.4	49 32 13	9.62	0.43	F3 V	8.616[e]	...	29.59	56	I
HE 965.....	+48°943	21672	3 31 53.8	48 44 08	6.62	−0.03	B8 V	6.646[e]	...	29.48	225	P, I
HE 968.....	...	...	3 31 54.1	48 31 40	10.41	0.57	F8 V	9.032[e]	...	30.21	38	P, I
HE 970.....	+48°944	...	3 31 55.6	48 35 03	8.19	0.19	A4 V	7.768[e]	...	<28.90	120	P, I
HE 985.....	+47°847	21699	3 32 08.5	48 01 26	5.46	−0.1	B8 IIImnp	5.631[e]	...	<28.95	50	I
AP 193.....	...	...	3 32 10.2	49 08 29	12.28	0.85	...	9.903[e]	29.75	30.3	64	H
AP 194.....	...	...	3 32 14.9	46 39 23	12.02	0.74	...	10.129	...	...	<10	I

TABLE 1—*Continued*

Object	BD	HD	R.A.[a] (J2000)	Decl.[a] (J2000)	V[a]	$B-V$[a]	Sp.[a]	K	log L_X[b]	log L_X[c]	$v \sin i$ (km s^{-1})	Tel.[d]
AP 118	...	...	3 32 30.6	49 10 35	12.06	0.81	...	9.808[e]	30.01	30.14	160	H
AP 199	...	...	3 32 44.4	47 41 36	12.10	0.98	...	9.602	...	29.99	23	I
AP 201	...	...	3 32 51.1	49 50 44	13.08	...	K5	10.236[e]	29.85	<29.84	12	H
HE 1082.....	+48°949	21931	3 34 13.0	48 37 03	7.37	0.02	B9 V	7.212[e]	...	<29.43	205	P, I
HE 1100.....	...	...	3 34 28.6	47 04 25	11.50	0.4	...	9.557[e]	...	...	<10	I
AP 213	...	...	3 34 39.4	48 18 44	11.55	0.83	G6	9.580[e]	...	<29.35	0	P, I
HE 1101.....	...	...	3 35 08.6	49 44 40	11.25	0.69	G4	9.441[e]	30.56	...	35	P, I
HE 1153.....	+46°773	22136	3 35 58.5	47 05 28	6.878	−0.023	B8 V	6.952	...	...	25	I
AP 225	...	...	3 36 22.0	49 09 21	11.83	0.78	...	9.706[e]	30.61	...	138	I
HE 1185.....	...	...	3 36 57.6	48 44 47	11.19	0.723	F7	9.405	...	...	<10	P, I
HE 1259.....	+47°865	22401	3 38 15.6	47 34 37	7.46	0.01	A0 V	7.415	...	...	45	I
AP 256	...	...	3 43 38.5	46 03 48	11.79	0.81	...	9.689[e]	...	...	10	I
AP 264	...	...	3 50 27.8	47 49 06	12.12	1.01	...	9.834[e]	...	...	14	I

NOTE.—Units of right ascension are hours, minutes, and seconds, and units of declination are degrees, arcminutes, and arcseconds. SIMBAD nomenclature: AP *nnn* = Cl* Melotte 20 AP *nnn*, HE *nnnn* = Cl Melotte 20 *nnnn*.

[a] C. F. Prosser (ftp://cfa-ftp.harvard.edu/pub/stauffer/clusters) or SIMBAD.

[b] Prosser et al. 1996.

[c] Randich et al. 1996.

[d] (I) IRTF; (P) Palomar; (K) Keck; (H) *HST*.

[e] Not in 2MASS database.

tion limits of the singles. The ΔF140W values are reported, but in order to express the magnitude differences in terms of mass ratios, the ΔF140W values were converted to ΔJ based on a relation derived from the α Per single stars given in Appendix B.

4. RESULTS

4.1. *Binary Star Detections and Single-Star Detection Limits for α Per and Praesepe Members*

The majority of the detected binaries and multiples are newly resolved by this survey. Of the 209 (100 Praesepe, 109 α Per) stars observed with the speckle and shift-and-add techniques, 22 are resolved as binaries; 12 of these systems are new detections. The Praesepe survey accounts for 12 of the binaries, and the remaining 10 binaries are α Per members. Among the extreme properties of the detected binaries are a separation as small as 0.″053 and a K-magnitude difference as large as 4.5. Of the 33 α Per members observed with *HST*, 17 binaries and one quadruple are imaged, with all except one newly resolved. Many of these potential companions, however, are very faint and are beyond the dynamic range of the ground-based data set. Tables 4A, 4B, and 5 provide the properties of all the detected binaries and notes about previous measurements, which are described in Appendix A. The α Per binaries are divided into two sets, those with stellar companions (Table 4A) and those with candidate substellar companions (Table 4B). Table 5 lists all the Praesepe binaries, since all are in the stellar mass range. The analysis of the binary properties is confined to the systems with stellar companions.

Each of the systems listed in either Table 4A or Table 5 is assumed to be a physically associated pair, since the small separation coverage and limited dynamic range of the surveys restrict the probability of a chance superposition. Based on the number of stars recorded on the Schmidt plates in the region of α Per, 7×10^{-4} arcsec^{-2} (Prosser 1992), the chance-alignment probability is only ~1% for the IRTF field of view. Since the Schmidt plates are sensitive to stars fainter than the average detection limit of this IR survey, this is a conservative estimate. Praesepe is located at a higher Galactic latitude than α Per, 32° compared with −7°, making the probability of a chance alignment considerably smaller for binaries in Praesepe.

For the single stars, Tables 6 (α Per) and 7 (Praesepe) give the detection limits for companions at a separation of 0.″15; these tables also include notes about previous measurements. As explained in § 3, many stars observed with speckle at Palomar were reobserved at the IRTF with a more limited shift-and-add data set; for these targets, the limit at 0.″15 is determined from the Palomar data, but the IRTF observing date is also listed in Tables 6 and 7 to indicate the larger separation-range coverage. These detection limits for the unresolved stars are used to quantify the sensitivity of the survey and to define the complete region in the next subsection. The median detection limits for several separations are summarized in Figure 1, which also shows the binaries detected in each cluster.

4.2. *α Per and Praesepe Survey Sensitivity*

Since the α Per and Praesepe members were observed with several telescope systems, the range of separation and magnitude difference is limited before combining the data sets. Because the observations were made with telescopes ranging in diameter from 3 to 10 m, the resolution limit is not the same for all targets. The largest value of λ/D is 0.″15, for the 3 m IRTF at 2.2 μm, and this separation is chosen as the inner separation cutoff for the complete region. The widest separation considered is 3.″4, one-half of the field of view of the IRTF camera. Of the 242-star α Per/Praesepe sample, only the 18 stars observed exclusively with Keck and 20 targets observed only at Palomar do not cover the entire separation range of 0.″15 to 3.″4. The Keck data are limited to separations less than 2.″63, while the Palomar data only extend to 1.″07. Given the 5 pc difference in cluster distances and the 0.″15–3.″4 angular range, the common projected separation range 26 to 581 AU is considered the complete separation range. The imposition of a separation range excludes seven binaries, leaving 26 systems with appropriate sepa-

TABLE 2

PRAESEPE SAMPLE

Name	BD	HD	R.A.[a] (J2000)	Decl.[a] (J2000)	V[a]	$B-V$[a]	Sp.[a]	K	log L_X[b]	Tel.[c]
II 490	...	...	8 27 59	22 06 08	9.67	0.45	...	8.693	...	I
II 582	...	...	8 29 54	22 26 31	9.88	0.49	...	8.823	...	I
A 70	...	...	8 31 13	18 09 21	9.86	0.46	...	8.767	...	I
I 563.....	...	...	8 33 27	16 35 19	10.11	0.5	...	8.849	...	I
A 365	...	...	8 35 17	20 33 49	8.42	0.26	...	7.779	...	I
JS 88	+20°2119	...	8 35 28.1	20 11 47	10.34	0.59	...	8.924	...	I
KW 534.....	+20°2125	72942	8 36 17.47	20 20 29.43	7.53	0.22	Am	7.185	...	I
KW 536.....	+19°2045	...	8 36 29.898	18 57 56.77	9.42	0.51	F6 V	8.329	...	I
KW 538.....	+19°2047	73045	8 36 48.049	18 52 57.88	8.62	0.38	Am	7.991	...	I
KW 16	+20°2128	73081	8 37 02.074	19 36 16.98	9.16	0.51	F6 V	8.059	28.90	I
KW 38	+20°2131	73161	8 37 33.866	20 00 48.99	8.69	0.33	F0 Vn	7.944[d]	...	I
KW 40	+20°2132	73174	8 37 37.031	19 43 58.19	7.79	0.22	Am	7.255[d]	29.15	I
KW 45	+20°2133	73175	8 37 40.743	19 31 05.97	8.25	0.23	F0 Vn	7.617[d]	...	P, I
KW 47	+19°2052	...	8 37 42.408	19 08 01.34	9.82	0.5	F4 V	8.713[d]	...	I
KW 50	+19°2053	73210	8 37 46.799	19 16 01.73	6.75	0.19	A5 V	6.354[d]	...	P, I
A 609	...	...	8 38 08	17 03 03	9.77	0.44	...	8.720	...	I
KW 100.....	...	...	8 38 24.351	20 06 21.47	10.55	0.58	G0 V	9.164[d]	...	K
KW 114.....	+20°2138	73345	8 38 37.909	19 59 22.97	8.14	0.21	F0 V	7.653	...	P, I
KW 124.....	+20°2139	73397	8 38 46.976	19 30 02.93	9	0.32	F4 V	8.273	...	P, I
KW 142.....	+20°2140	...	8 39 02.876	19 43 28.63	9.31	0.49	F7 V	8.135	29.30	P, I
KW 143.....	+20°2141	73430	8 39 03.628	19 59 58.92	8.31	0.23	A9 V	7.780	...	P, I
KW 146.....	+20°2142	73429	8 39 05.279	20 07 01.5	9.39	0.4	F5 V	8.432	...	I
KW 150.....	+20°2143	73449	8 39 06.148	19 40 36.18	7.45	0.25	A9 Vn	6.728	...	P, I
KW 154.....	+20°2144	73450	8 39 09.131	19 35 32.25	8.5	0.25	A9 V	7.889	...	P, I
KW 155.....	+20°22143	...	8 39 10.182	19 40 42.01	9.42	0.41	F6	8.449	...	I
KW 181.....	+19°2061	...	8 39 25.017	19 27 33.34	10.47	0.59	F7 V	9.039	28.90	K
KW 182.....	+20°2146	...	8 39 30.455	20 04 08.3	10.31	0.68	F8 V	8.827	28.78	I
KW 203.....	+20°2148	73574	8 39 42.835	20 05 10.28	7.73	0.22	A5 V	7.190	...	P, I
KW 253.....	+20°2158	73665	8 39 36.574	20 54 36.07	6.39	0.98	G8 III	...	...	P
KW 204.....	+20°2149	73575	8 39 42.715	19 46 42.3	6.67	0.25	F0 III	6.027	...	P, I
KW 207.....	...	...	8 39 44.696	19 16 30.38	7.67	0.2	A7 Vn	7.127	...	P, I
KW 212.....	+20°2150	73598	8 39 50.762	19 32 26.76	6.59	0.96	K0 III	...	29.90	P
KW 217.....	...	...	8 39 52.369	19 18 45.15	10.23	0.51	F5 V	9.086	29.08	K
KW 218.....	+21°1882	73597	8 39 54.374	20 33 36.9	9.36	0.44	F6 V	8.436	...	I
KW 222.....	+20°2151	...	8 39 55.109	20 03 53.73	10.11	0.49	F4 V	8.985	29.00	K
KW 224.....	+20°2152	73618	8 39 56.527	19 33 10.5	7.32	0.19	Am	6.809	29.94	P, I
KW 229.....	+20°2153	73619	8 39 57.811	19 32 29.1	7.54	0.25	Am	7.030	29.94	P, I
KW 227.....	+19°2066	73641	8 39 58.103	19 12 05.48	9.49	0.41	F6 V	8.533	...	I
KW 226.....	+20°2154	73616	8 39 58.422	20 09 29.36	8.89	0.32	F2 V	8.113	...	P, I
KW 232.....	+20°2155	73617	8 39 59.119	20 01 52.87	9.23	0.39	F5 V	8.248	...	I
KW 238.....	...	...	8 40 00.66	19 48 23.17	10.3	0.51	F6 V	9.091	29.00	K
KW 239.....	+20°2156	73640	8 40 01.333	20 08 07.91	9.67	0.44	F6 V	8.599	29.00	I
KW 244.....	+19°2068	...	8 40 01.742	18 59 59.05	9.98	0.62	F8 V	8.704	30.05	I
KW 250.....	+20°2157	...	8 40 04.942	19 43 44.94	9.79	0.47	F6 V	8.693	...	I
KW 258.....	...	...	8 40 06.308	19 27 14.64	10.24	0.57	F6 V	8.893	...	I
KW 265.....	+20°2159	73666	8 40 11.506	19 58 16.1	6.61	0.01	A1 V	6.543	...	P, I
KW 268.....	+20°2160	...	8 40 12.354	19 38 21.92	9.89	0.48	F5 V	8.698	...	I
KW 271.....	+20°2161	...	8 40 15.396	19 59 39.13	8.81	0.32	F2 V	8.064	...	I
KW 275.....	+20°2162	...	8 40 17.658	19 47 14.86	9.96	0.58	F8 V	8.628	...	I
KW 276.....	+20°2163	73711	8 40 18.135	19 31 54.93	7.54	0.16	F0 III	7.187	29.04	P, I
KW 284.....	+19°2069	73712	8 40 20.178	19 20 56.07	6.78	0.26	A9 V	6.063	...	P, I
KW 279.....	+20°2165	73709	8 40 20.796	19 41 11.97	7.7	0.2	F2 III	7.290	...	P, I
KW 283.....	+20°2166	73710	8 40 21	19 40 25	6.44	1.02	G9 III	...	29.04	P
KW 282.....	+20°2164	...	8 40 22.355	20 06 23.97	10.08	0.51	F2 III	8.837	...	K
KW 286.....	+20°2168	73730	8 40 23.508	19 50 05.67	8.02	0.19	F2 III	7.599	...	P, I
KW 293.....	...	...	8 40 25.575	19 28 32.44	9.85	0.47	...	8.796	...	I
KW 295.....	+20°2170	...	8 40 26.18	19 41 10.96	9.37	0.42	F6 V	8.381	28.90	I
KW 292.....	+20°2169	73729	8 40 26.791	20 10 55	8.18	0.3	F2 Vn	7.426	...	P, I
KW 300.....	+20°2171	73731	8 40 27.058	19 32 41.31	6.3	0.17	A5m	5.880	28.70	P, I
KW 318.....	+19°2072	73746	8 40 32.994	19 11 39.29	8.65	0.29	F0 V	7.965	...	P
KW 323.....	+19°2073	73763	8 40 39.277	19 13 41.48	7.8	0.22	A9 V	7.249	...	P
KW 328.....	+20°2172	73785	8 40 43.26	19 43 09.45	6.85	0.2	A9 III	6.348	28.90	P, I
KW 332.....	+19°2074	...	8 40 46.116	19 18 34.26	9.55	0.43	F6 V	8.566	...	I
KW 340.....	+20°2173	73798	8 40 52.523	20 15 59.19	8.48	0.26	F0 Vn	7.822	...	P

TABLE 2—*Continued*

Name	BD	HD	R.A.[a] (J2000)	Decl.[a] (J2000)	V[a]	$B-V$[a]	Sp.[a]	K	log L_X[b]	Tel.[c]
KW 341.....	...	...	8 40 52.564	19 28 59.18	10.3	0.52	F7 V	9.067	...	K
KW 348.....	+20°2175	73819	8 40 56.337	19 34 48.96	6.78	0.17	A6 Vn	6.293	...	P, I
KW 350.....	+20°2174	73818	8 40 56.962	19 56 05.51	8.71	0.32	Am	8.062	...	I
KW 365.....	+19°2076	...	8 41 07.399	19 04 16.06	10.18	0.64	G0	8.689	...	I
KW 371.....	+20°2176	...	8 41 10.053	19 30 31.72	10.11	0.5	F6 V	8.952	...	P
KW 370.....	+20°2177	73854	8 41 10.708	19 49 46.04	9.04	0.36	F5 V	8.212	29.04	P
KW 375.....	+20°2179	73872	8 41 13.816	19 55 18.9	8.33	0.2	A5 V	7.796	29.66	P, I
KW 385.....	+19°2078	73890	8 41 18.437	19 15 38.97	7.92	0.24	A7 Vn	7.328	...	P, I
KW 396.....	+20°2180	...	8 41 26.996	19 32 32.46	9.83	0.46	F4 V	8.751	...	I
KW 411.....	+19°2080	73937	8 41 36.241	19 08 33.28	9.32	0.39	F4 V	8.373	...	I
KW 416.....	+20°2183	...	8 41 42.335	19 39 37.65	9.59	0.41	F6 V	8.512	...	I
KW 418.....	+20°2184	...	8 41 43.853	20 13 36.26	10.47	0.56	F7	9.194	...	K
KW 421.....	+19°2081	...	8 41 45.535	19 16 01.91	10.17	0.52	...	8.958	...	K
KW 429.....	+20°2186	73993	8 41 53.177	20 09 33.59	8.53	0.3	F2 Vn	7.807	...	P, I
KW 439.....	+19°2082	73994	8 41 57.857	18 54 41.84	9.45	0.39	F5 V	8.484	...	I
KW 445.....	+19°2083	74028	8 42 06.54	19 24 40.34	7.96	0.21	A7 V	7.428	...	P, I
KW 449.....	+19°2084	74050	8 42 10.848	18 56 03.42	7.91	0.21	A7 Vn	7.359	...	I
KW 454.....	...	...	8 42 15.528	19 41 15.22	9.88	0.46	...	8.782	...	K
KW 458.....	+20°2189	...	8 42 20.166	20 02 11.31	9.71	0.55	F6 V	8.497	...	I
KW 459.....	+20°2191	74058	8 42 21.646	20 10 53.42	9.23	0.39	F3 Vn	8.284	29.51	P
JS 495.....	+18°2020	...	8 42 36.8	18 23 20	10.13	0.52	...	8.994	...	I
KW 472.....	+20°2192	...	8 42 40.762	19 32 35.13	9.77	0.45	F2 III	8.758	...	I
KW 478.....	+20°2193	...	8 42 44.442	19 34 47.5	9.68	0.43	F6 V	8.664	...	I
A 1196.....	...	...	8 42 53	20 49 11	8.84	0.33	...	8.106	...	I
KW 496.....	+19°2088	74186	8 43 07.091	19 04 06.11	9.56	0.52	F8 V	8.376	...	I
JS 532.....	...	...	8 43 22.7	21 40 18	10.59	0.71	...	9.027	29.04	I
KW 515.....	+20°2196	...	8 43 35.601	20 11 22.07	10.13	0.51	F6 V	8.914	...	I
KW 549.....	+19°2089	...	8 43 48.197	18 48 02.8	10.11	0.51	F8	8.965	...	I
KW 553.....	+20°2198	...	8 44 07.369	20 04 36.5	10.15	0.45	...	9.081	...	K
JS 589.....	...	...	8 45 14.7	20 59 51	9.46	0.42	...	8.498	...	I
A 1480.....	...	...	8 45 18	18 53 27	9.51	0.46	...	8.625	...	I
A 1501.....	...	...	8 45 29	20 23 38	8.51	0.28	...	7.888	...	I
JS 600.....	...	...	8 45 30.5	20 35 24	9.82	0.46	...	8.797	...	I
A 1528.....	...	...	8 45 47	19 03 01	8.03	0.24	...	7.546	...	I
A 1565.....	...	...	8 46 11	18 10 42	8.27	0.23	...	7.677	...	I
A 1583.....	...	...	8 46 15	19 42 30	8.39	0.24	...	7.813	...	I

NOTE.—SIMBAD nomenclature: KW *nnn* = Cl* NGC 2632 KW *nnn*, A *nnnn* = Cl* NGC 2632 Art *nnnn*.
[a] C. F. Prosser (ftp://cfa-ftp.harvard.edu/pub/stauffer/clusters) or SIMBAD.
[b] Randich & Schmitt 1995; Stern et al. 1995.
[c] (I) IRTF; (P) Palomar; (K) Keck.
[d] Not in 2MASS database.

TABLE 3
OBSERVING SUMMARY

Telescope	Date	Obs.	Technique
		α Per	
Palomar	1997 Oct 8	45	Speckle
IRTF	1997 Dec 4–9	43/3	Speckle + shift-and-add/shift-and-add only
	1998 Feb 18–20	14/33	Speckle + shift-and-add/shift-and-add only
HST.....	1998 Feb 28; Jul 25; Aug 8, 23, 26–28, 31	33	Imaging
Keck	1999 Jan 6–7	7	Speckle + shift-and-add
		Praesepe	
Palomar	1995 Nov 12–13	8	Speckle
	1996 Jan 8–9	26	Speckle
IRTF	1998 Feb 18–20	20/23	Speckle + shift-and-add/shift-and-add only
	1999 Feb 13–15	35	Speckle + shift-and-add
Keck	1999 Jan 6–7	11	Speckle + shift-and-add

TABLE 4A
α PERSEI STELLAR BINARIES

Object	Telescope	Date	Separation (arcsec)	P.A. (deg)	ΔK/ ΔF140w	M_1 ($M_\odot$)	M_2 ($M_\odot$)	q	No. Comp.	Notes[a]
AP 60	*HST*	1998 Aug 27	0.053 ± 0.004	350 ± 3	0.12 ± 0.02	0.59	0.57	0.98	1	New
HE 935	Palomar	1997 Oct 8	0.056 ± 0.006	6 ± 9	0.3 ± 0.3	0.97	0.91	0.94	1	New
HE 965	Palomar	1997 Oct 8	0.117 ± 0.004	350 ± 6	2.5 ± 0.2	2.61	1.04	0.40	2	New; ? (M&A)
HE 581	Palomar	1997 Oct 8	0.120 ± 0.003	17 ± 4	2.8 ± 0.2	2.40	0.90	0.38	1	New; S (M&A)
AP 139	Keck	1999 Jan 7	0.19 ± 0.01	72 ± 4	3.5 ± 0.1	0.89	0.26	0.30	1	New
HE 285	Palomar	1997 Oct 8	0.214 ± 0.005	320 ± 1	1.25 ± 0.03	1.84	1.17	0.63	1	B? (P)
AP 149AB	*HST*	1998 Aug 26	0.327 ± 0.003	97.7 ± 0.4	0.956 ± 0.009	0.88	0.72	0.82	1	New
AP 98	*HST*	1998 Feb 28	0.332 ± 0.008	298 ± 1	2.93 ± 0.08	0.79	0.31	0.39	1	New
HE 696	IRTF	1997 Dec 8	0.43 ± 0.01	184 ± 4	2.5 ± 0.1	0.89	0.47	0.53	1	New
AP 41	*HST*	1998 Aug 26	0.532 ± 0.007	315.26 ± 0.09	2.770 ± 0.007	0.88	0.48	0.55	1	New
AP 201	*HST*	1998 Aug 30	0.544 ± 0.002	337.4 ± 0.3	1.40 ± 0.03	0.77	0.58	0.75	1	New
HE 835	IRTF	1997 Dec 4	0.67 ± 0.01	34 ± 1	1.96 ± 0.03	4.87	2.37	0.49	1	S (M&A), B (ADS) 0.″68
AP 17	*HST*	1998 Aug 23	0.969 ± 0.001	8.15 ± 0.09	2.78 ± 0.03	0.66	0.19	0.29	1	New
HE 780	Keck	1999 Jan 7	1.38 ± 0.03	317 ± 1	2.88 ± 0.01	1.90	0.76	0.40	1	New
AP 121	IRTF	1997 Dec 6	1.44 ± 0.03	31.2 ± 2	3.5 ± 0.2	0.86	0.24	0.28	1	New
HE 828	IRTF	1997 Dec 6	1.63 ± 0.03	234 ± 1	2.60 ± 0.06	0.89	0.44	0.50	2	New; B (P) 10.″5
AP 75	*HST*	1998 Aug 27	1.910 ± 0.005	79.0 ± 0.3	5.107 ± 0.008	0.77	0.10	0.13	1	New
AP 193	*HST*	1998 Aug 28	2.102 ± 0.005	50.9 ± 0.4	5.221 ± 0.008	0.88	0.12	0.14	1	New
AP 6	*HST*	1998 Aug 23	2.876 ± 0.001	263.47 ± 0.08	1.51 ± 0.09	0.60	0.32	0.54	1	New
AP 106	*HST*	1998 Aug 23	4.571 ± 0.002	17.06 ± 0.08	2.34 ± 0.02	0.76	0.41	0.54	1	B (P) 4.″5
AP 108	*HST*	1998 Aug 31	4.947 ± 0.004	50.61 ± 0.06	4.76 ± 0.01	0.80	0.13	0.16	1	New

[a] Single (S) or binary (B), and separation: (M&A) Morrell & Abt 1992; (P) Prosser 1992; (ADS) Aitken 1932.

TABLE 4B
α PERSEI FAINT DOUBLES

Object	Telescope	Date	Separation (arcsec)	P.A. (deg)	ΔF140W	M_1 ($M_\odot$)	M_2 ($M_\odot$)	q	No. Comp.
AP 72	*HST*	1998 Jul 25	3.045 ± 0.003	35.4 ± 0.2	8.471 ± 0.006	0.78	0.03	0.037	1
AP 15	*HST*	1998 Aug 31	3.512 ± 0.001	197.8 ± 0.3	7.70 ± 0.04	0.73	0.03	0.047	1
AP 112	*HST*	1998 Aug 27	4.402 ± 0.006	337.42 ± 0.03	6.557 ± 0.007	0.73	0.05	0.073	1
AP 101	*HST*	1998 Aug 23	4.999 ± 0.001	160.62 ± 0.06	5.68 ± 0.09	0.75	0.08	0.104	1
AP 149AC	*HST*	1998 Aug 26	5.05 ± 0.01	160.2 ± 0.1	7.46 ± 0.01	0.94	0.06	0.064	3
AP 149AD	*HST*	1998 Aug 26	5.381 ± 0.002	7.842 ± 0.002	8.46 ± 0.06	0.94	0.04	0.044	...
AP 86	*HST*	1998 Aug 27	5.412 ± 0.002	66.3 ± 0.1	7.34 ± 0.08	0.70	0.04	0.052	1
AP 95	*HST*	1998 Feb 28	6.087 ± 0.002	188.52 ± 0.05	7.186 ± 0.005	0.88	0.06	0.067	1
AP 19	*HST*	1998 Aug 26	7.287 ± 0.003	49.88 ± 0.02	6.77 ± 0.02	0.94	0.08	0.083	1

rations. One Praesepe binary—KW 284—and four α Per systems—HE 935, AP 60, HE 965, and HE 581—have separations smaller than the inner cutoff. Two additional α Per *HST* binaries with companions bright enough to be above the stellar limit—AP 108 and AP 106—have separations larger than the outer cutoff.

At a separation of 0.″15, the median speckle detection limit is $\Delta K = 3.6$ mag, which corresponds to a mass ratio limit of $q \sim 0.3$. Although the *HST* data are not as sensitive at the closest separations, the sensitivity is comparable or higher for most of the separation range. No corrections are applied, since the *HST* observations represent only ~15% of the α Per/Praesepe sample and only ~5% of the combined cluster sample analyzed in § 6.2. Two different cutoffs are used in the analysis. The discussion about the frequency of companions (CSF) involves a cutoff based on the observed ΔK and includes the 23 binaries with appropriate separations and with $\Delta K \leq 4$, while the discussion of the mass ratio distribution imposes a more conservative cutoff based on the derived mass ratio value and only includes the 19 systems with separations between 26 and 581 AU and $q \geq 0.4$. The mass ratio limit is not unique for a given ΔK, since the mass-magnitude relation involves several functions (Henry & McCarthy 1993; Patience et al. 1998); the $\Delta K = 4$ limit is approximately a mass ratio limit of $q \sim 0.25$, and the mass ratio limit of $q = 0.40$ translates into a magnitude limit of approximately $\Delta K \sim 3$ (see Appendix B for details). Since the stars in the samples represent different masses with spectral types from B to K, a mass ratio limit corresponds to companion mass detection limits that scale with the target star's mass. Within the complete separation range, one Praesepe binary—KW 212—and two α Per binaries—AP 75 and AP 193—have mass ratios below 0.25. One additional Praesepe pair—KW 282—and four additional α Per pairs—AP 98, 17, 139, and 121—have mass ratios between 0.25 and 0.40.

4.3. *Comparison Surveys*

In addition to the current α Per and Praesepe surveys, a number of multiplicity surveys have been conducted in regions with different ages. The current results are enhanced

TABLE 5
PRAESEPE BINARIES

Object	Telescope	Date	Separation (arcsec)	P.A. (deg)	ΔK	M_1 (M)	M_2 (M)	q	No. Comp.	Notes[a]
KW 284.....	Palomar	1995 Nov 12	0.104 ± 0.002	159 ± 3	1.7 ± 0.1	3.00	1.61	0.54	1	B (M) 0.″054, B (AW99)
KW 275.....	IRTF	1998 Feb 20	0.198 ± 0.004	91 ± 1	0.06 ± 0.06	0.98	0.96	0.99	1	S (B91), B (MM99)
KW 232.....	IRTF	1998 Feb 18	0.27 ± 0.05	22 ± 5	2.5 ± 0.4	1.40	0.68	0.49	1	New; S (M)
KW 458.....	IRTF	1998 Feb 19	0.279 ± 0.005	167 ± 1	0.66 ± 0.04	1.12	0.91	0.82	1	S (B91), B (MM99)
A 1565.....	IRTF	1999 Feb 13	0.330 ± 0.008	352 ± 2	1.16 ± 0.04	1.59	1.04	0.65	1	New
KW 365.....	IRTF	1998 Feb 20	0.340 ± 0.006	72 ± 1	0.80 ± 0.06	1.06	0.85	0.81	2	B (B91) 21 days, T (MM99)
KW 282.....	Keck	1999 Jan 6	0.383 ± 0.008	153 ± 1	4.0 ± 0.1	1.16	0.33	0.28	1	New
KW 203.....	Palomar	1996 Jan 8	0.499 ± 0.009	40 ± 2	0.80 ± 0.03	1.83	1.37	0.75	1	B (P&W) 0.″326, B (M) 0.″550, S (AW99)
KW 212.....	Palomar	1995 Nov 13	0.80 ± 0.05	233 ± 1	4.5 ± 0.3	Giant	...	...	1	B (P&W) 0.″346, B (M) 0.″492, S (AW99)
KW 250.....	IRTF	1998 Feb 20	0.90 ± 0.06	208 ± 1	2.90 ± 0.04	1.20	0.56	0.46	1	New; S (MM99)
KW 224.....	IRTF	1998 Feb 19	0.96 ± 0.02	250 ± 1	2.30 ± 0.01	2.35	1.01	0.43	2	B (IDS) 1.″4, S (P&W), S (M), B (B&C), B (AW99)
KW 385.....	IRTF	1998 Feb 20	2.14 ± 0.04	14 ± 1	1.51 ± 0.03	1.86	1.07	0.58	1	B (ADS) 2.″4, S (M)

[a] Single (S), binary (B), or triple (T), and separation or period: (M) Mason et al. 1993; (AW99) Abt & Willmarth 1999; (B91) Bolte 1991; (MM99) Mermilliod & Mayor 1999; (P&W) Peterson & White 1984; (IDS) Jeffers & van den Bos 1963; (B&C) Burkhart & Coupry 1989; (ADS) Aitken 1932.

by placing them in the context of these previous studies. In order to best compare the current surveys with previous work, this section describes the detections, sensitivity, and separation-range coverage of these investigations of nearby star-forming regions, additional clusters, and the solar neighborhood reported in the literature. The discussion of the α Per and Praesepe results and how they compare with other samples and with theoretical expectations begins in § 5.

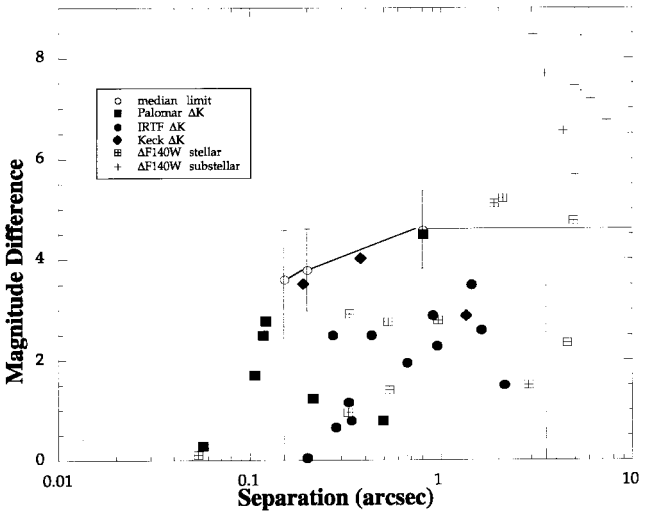

FIG. 1.—Binaries and detection limits. The detected binaries in the α Per and Praesepe samples are plotted with a different symbol depending upon the telescope used; *HST* companions are further differentiated based on the companion mass. Open circles connected by solid lines delineate the median detection limits of the sample, with the error bars indicating the standard deviation of the limits. Dashed lines mark the bounds of separation range considered for the complete sample. Since the diffraction limit of the IRTF is 0.″15, this separation is taken as the lower limit for the complete range, although a number of binaries are resolved to separations as little as 0.″027 by Keck, Palomar, and *HST*. The outer limit is 3.″3 for α Per and 3.″4 for Praesepe, with the slight difference due to the 5 pc variation in the cluster distances.

4.3.1. *Open Clusters*

The results of two previous surveys of open clusters—the Pleiades and the Hyades—are included in much of the analysis of binary star properties. An adaptive optics (AO) survey of 143 Pleiades G and K dwarfs (mass range ~0.6–1.1 $M_\odot$) (Bouvier et al. 1997) provides an excellent comparison sample with an intermediate age between α Per and Praesepe. Since the Pleiades are slightly closer ($D = 132$ pc; Pinsonneault et al. 1998), the separation range 26 to 581 AU corresponds to 0.″20 to 4.″40, a subset of the Pleiades survey that spanned 0.″08 to 6.″0. Within the separation range of 26 to 581 AU and $\Delta K < 4.0$ mag, there are 17 Pleiades companions, all of which have colors consistent with cluster membership. Overall, the detection limits of the Pleiades survey are quite similar to the speckle survey presented here. Specifically, the Pleiades observations are less sensitive (by 0.5–1.5 mag) over the small separation range from 0.″20 to 0.″4 and slightly more sensitive (by 0.5–1.0 mag) at separations wider than ~1.″0. Each of the Pleiades binaries in the 26–581 AU and $K < 4.0$ range would have been detected by the α Per and Praesepe speckle surveys. Conversely, all but three of the Praesepe and α Per binaries in the 26–581 AU and $\Delta K < 4.0$ range would have been detected by the Pleiades survey, and the largest-ΔK systems in α Per and Praesepe are only 0.5–1.0 mag beyond the Pleiades detection limit.

Another open cluster, the Hyades, has also been searched with high-resolution techniques for companions to 162 A to early K stars (mass range ~0.6–2.4 $M_\odot$) (Patience et al. 1998). Its closer distance ($D = 46.3$ pc; Perryman et al. 1998), however, translates the observed 0.″1–1.″07 angular separation range into 5 to 50 AU. There are 23 binaries in the Hyades sample with $\Delta K < 4.0$ and projected separations from 5 to 50 AU. The Hyades data were taken with the same Palomar speckle camera and therefore have a similar companion sensitivity over this smaller projected separation range. Although there is little projected linear separation range overlap with the current survey, the proportion of Hyades binaries in the 5–50 AU range is only slightly higher than that of the α Per, Praesepe, and Pleiades clusters in the 26–581 AU range. To increase the sample size, the distribution of Hyades speckle binary properties is combined with the other cluster data in order to study mass ratio distribu-

TABLE 6

α PERSEI SINGLE STARS

Name	Telescope	Date	$\Delta K_{\rm lim}$ at 0.″15	$q_{\rm lim}$	No. Comp.	Notes[a]
HD 18537	IRTF	1998 Feb 18	2.87	0.34	0	B (ADS) 12.″18
HD 18538	IRTF	1998 Feb 18	2.03	0.45	0	
HE 12.....	Palomar	1997 Oct 8	4.2	0.26	0	
	IRTF	1998 Feb 18				
HE 56.....	Palomar	1997 Oct 8	3.76	0.31	0	
	IRTF	1998 Feb 18				
HE 92.....	IRTF	1997 Dec 6	2.49	0.51	0	
HE 93.....	IRTF	1997 Dec 6	1.98	0.60	0	
HE 94.....	Keck	1999 Jan 7	4.23	0.26	0	
HE 104.....	Palomar	1997 Oct 8	4.29	0.29	0	
	IRTF	1998 Feb 18				
HE 1082.....	Palomar	1997 Oct 8	4.25	0.27	0	S (M&A)
	IRTF	1998 Feb 19				
HE 1100.....	IRTF	1997 Dec 6	4.18	0.22	0	
HE 1101.....	Palomar	1997 Oct 8	4.18	0.22	0	
	IRTF	1998 Feb 20				
HE 1153.....	IRTF	1997 Dec 5	3.54	0.31	0	S (M&A)
HE 1185.....	Palomar	1997 Oct 8	4.27	0.22	0	
	IRTF	1998 Feb 20				
HE 1259.....	IRTF	1997 Dec 5	2.7	0.40	0	S (M&A)
HE 135.....	IRTF	1997 Dec 8	1.95	0.54	0	
HE 143.....	Palomar	1997 Oct 8	4.45	0.22	1	B (M, P)
	IRTF	1998 Feb 18				
HE 151.....	IRTF	1997 Dec 8	2.6	0.45	0	
HE 167.....	Palomar	1997 Oct 8	3.73	0.33	0	
	IRTF	1997 Dec 8				
HE 212.....	Palomar	1997 Oct 8	3.54	0.32	0	
	IRTF	1998 Feb 18				
HE 220.....	IRTF	1997 Dec 8	3.92	0.33	0	
HE 270.....	IRTF	1997 Dec 6	2.44	0.51	0	
HE 299.....	IRTF	1997 Dec 6	3.08	0.40	0	
HE 309.....	Keck	1999 Jan 7	4.87	0.17	0	
HE 314.....	IRTF	1998 Feb 18	2.07	0.50	1	B (P)
HE 333.....	Palomar	1997 Oct 8	3.92	0.28	0	
	IRTF	1998 Feb 18				
HE 334.....	Palomar	1997 Oct 8	4.01	0.28	0	
	IRTF	1998 Feb 18				
HE 338.....	Palomar	1997 Oct 8	3.89	0.32	0	
	IRTF	1998 Feb 18				
HE 350.....	Palomar	1997 Oct 8	3.62	0.33	0	
	IRTF	1998 Feb 20				
HE 361.....	IRTF	1998 Feb 19	2.13	0.52	0	
HE 365.....	IRTF	1998 Feb 19	2.94	0.44	0	
HE 373.....	IRTF	1997 Dec 9	3.73	0.29	0	
HE 383.....	Palomar	1997 Oct 8	3.98	0.23	0	S (M&A)
	IRTF	1997 Dec 4				
HE 386.....	IRTF	1997 Dec 7	2.78	0.40	0	
HE 401.....	IRTF	1997 Dec 4	3.08	0.32	0	
HE 407.....	Palomar	1997 Oct 8	3.25	0.37	0	
	IRTF	1998 Feb 20				
HE 421.....	IRTF	1997 Dec 9	2.6	0.44	0	
HE 423.....	IRTF	1997 Dec 7	3.4	0.34	1	
HE 481.....	IRTF	1997 Dec 9	2.78	0.43	0	
HE 490.....	IRTF	1997 Dec 9	1.89	0.54	0	
HE 520.....	IRTF	1997 Dec 8	2.28	0.56	0	
HE 557.....	Palomar	1997 Oct 8	4.45	0.21	0	
HE 575.....	Palomar	1997 Oct 8	4.39	0.27	0	S (M&A)
	IRTF	1998 Feb 20				
HE 588.....	Palomar	1997 Oct 8	3.45	0.38	0	
	IRTF	1998 Feb 20				
HE 609.....	IRTF	1997 Dec 7	2.87	0.41	0	
HE 612.....	Palomar	1997 Oct 8	4.33	0.28	0	S (M&A)
	IRTF	1998 Feb 20				
HE 621.....	IRTF	1997 Dec 6	3.86	0.32	0	

TABLE 6—*Continued*

Name	Telescope	Date	$\Delta K_{\rm lim}$ at 0.″15	$q_{\rm lim}$	No. Comp.	Notes[a]
HE 625.....	Palomar	1997 Oct 8	3.76	0.31	0	S (M&A)
	IRTF	1998 Feb 20				
HE 632.....	IRTF	1997 Dec 6	2.5	0.49	0	
HE 639.....	Palomar	1997 Oct 8	3.73	0.33	0	
	IRTF	1998 Feb 20				
HE 651.....	IRTF	1997 Dec 7	2.87	0.41	0	
HE 665.....	Palomar	1997 Oct 8	3.25	0.38	0	B (IDS) 10.″6
HE 675.....	Palomar	1997 Oct 8	3.83	0.27	0	S (M&A)
	IRTF	1998 Feb 19				
HE 684.....	Palomar	1997 Oct 8	4.29	0.22	0	
	IRTF	1998 Feb 19				
HE 699.....	IRTF	1997 Dec 8	2.94	0.45	0	
HE 709.....	Palomar	1997 Oct 8	3.73	0.30	0	
	IRTF	1998 Feb 20				
HE 715.....	IRTF	1997 Dec 6	3.01	0.44	0	
HE 727.....	Palomar	1997 Oct 8	3.8	0.31	0	
	IRTF	1998 Feb 20				
HE 735.....	Palomar	1997 Oct 8	3.73	0.29	0	S (M&A)
	IRTF	1998 Feb 18				
HE 750.....	Palomar	1997 Oct 8	4.13	0.24	0	
	IRTF	1998 Feb 18				
HE 767.....	Palomar	1997 Oct 8	3.69	0.31	0	
	IRTF	1998 Feb 20				
HE 774.....	IRTF	1997 Dec 4	2.17	0.43	1	B (M&A) 21.7 days
HE 775.....	IRTF	1997 Dec 5	2.94	0.36	1	B (M&A) 21.2 days
HE 799.....	IRTF	1998 Feb 18	3.45	0.39	0	B (ADS) 6.″68
HE 810.....	Palomar	1997 Oct 8	3.76	0.25	0	S (M&A)
	IRTF	1998 Feb 18				
HE 817.....	Palomar	1997 Oct 8	3.62	0.31	1	B (M&A) 30.9 days
	IRTF	1998 Feb 18				
HE 831.....	Palomar	1997 Oct 8	4.03	0.29	0	S (M&A)
	IRTF	1997 Dec 5				
HE 833.....	IRTF	1998 Feb 18	2.6	0.49	0	
HE 841.....	Palomar	1997 Oct 8	3.08	0.44	0	
	IRTF	1998 Feb 20				
HE 848.....	Palomar	1997 Oct 8	3.45	0.39	1	B (M, P)
	IRTF	1998 Feb 20				
HE 862.....	Palomar	1997 Oct 8	4.98	0.20	0	
	IRTF	1998 Feb 20				
HE 868.....	Palomar	1997 Oct 8	4.03	0.28	1	? (M&A)
	IRTF	1998 Feb 20				
HE 885.....	IRTF	1997 Dec 6	2.17	0.49	0	
HE 904.....	IRTF	1997 Dec 5	3.98	0.25	0	S (M&A)
HE 906.....	IRTF	1997 Dec 5	4.08	0.32	0	
HE 917.....	Palomar	1997 Oct 8	3.92	0.27	0	
	IRTF	1998 Feb 19				
HE 921.....	IRTF	1997 Dec 7	4.41	0.26	0	
HE 931.....	IRTF	1997 Dec 7	3.49	0.37	0	
HE 944.....	IRTF	1997 Dec 6	4.06	0.29	0	
HE 955.....	Palomar	1997 Oct 8	4.11	0.27	1	? (M&A)
	IRTF	1997 Dec 5				
HE 968.....	Palomar	1997 Oct 8	4.2	0.24	0	
	IRTF	1998 Feb 19				
HE 970.....	Palomar	1997 Oct 8	4.35	0.28	0	
	IRTF	1998 Feb 20				
HE 985.....	IRTF	1997 Dec 5	3.98	0.24	0	S (M&A)
AP 14.....	IRTF	1997 Dec 9	2.6	0.45	0	
AP 20.....	*HST*	1998 Aug 27	1.06	0.80	0	
AP 21.....	*HST*	1998 Aug 27	1.04	0.78	0	
AP 25.....	*HST*	1998 Aug 26	1.06	0.80	0	
AP 28.....	*HST*	1998 Aug 27	1.07	0.80	0	
AP 37.....	*HST*	1998 Aug 27	1.1	0.80	0	
AP 43.....	*HST*	1998 Jul 25	1.07	0.80	0	
AP 56.....	*HST*	1998 Aug 27	1.07	0.80	0	
AP 63.....	Keck	1999 Jan 7	3.25	0.32	0	

TABLE 6—*Continued*

Name	Telescope	Date	$\Delta K_{\rm lim}$ at 0.″15	$q_{\rm lim}$	No. Comp.	Notes[a]
AP 70	*HST*	1998 Aug 27	1.06	0.80	0	
AP 78	*HST*	1998 Aug 27	1.05	0.80	0	
AP 90	IRTF	1997 Dec 6	3.2	0.38	0	
AP 92	*HST*	1998 Feb 28	1.06	0.71	0	
AP 97	IRTF	1997 Dec 9	2.48	0.49	0	
AP 100	*HST*	1998 Aug 8	1.06	0.80	0	
AP 102	IRTF	1998 Feb 20	2.78	0.43	0	
AP 104	IRTF	1998 Feb 20	1.98	0.57	0	
AP 110	Keck	1999 Jan 7	3.73	0.23	0	
AP 117	*HST*	1998 Aug 27	1.07	0.80	0	
AP 118	*HST*	1998 Aug 28	1.06	0.80	0	
AP 125	*HST*	1998 Feb 28	1.07	0.80	0	
AP 127	*HST*	1998 Jul 25	1.07	0.80	0	
AP 156*	IRTF	1998 Feb 19	2.17	0.57	0	
AP 158	IRTF	1997 Dec 8	3.8	0.25	0	
AP 173	Keck	1999 Jan 7	4.57	0.17	0	
AP 194	IRTF	1998 Feb 19	3.08	0.33	0	
AP 199	IRTF	1998 Feb 19	2.23	0.57	0	
AP 213	Palomar	1997 Oct 8	3.49	0.32	0	
	IRTF	1998 Feb 20				
AP 225	IRTF	1997 Dec 8	3.2	0.36	0	
AP 256	IRTF	1997 Dec 8	3.83	0.25	0	
AP 264	IRTF	1997 Dec 8	2.05	0.59	0	

[a] Single (S) or binary (B), and separation or period: (ADS) Aitken 1932; (M&A) Morrell & Abt 1992; (M) Mason et al. 1993; (P) Prosser 1992; (IDS) Jeffers & van den Bos 1963.

tions and the mass dependence of the binary properties (§ 6).

To extend the separation-range coverage of the cluster data, systems detected in spectroscopic studies are used to construct an overall binary separation distribution (§ 5.3). The Hyades have been thoroughly investigated with both speckle imaging (Mason et al. 1993; Patience et al. 1998) and spectroscopy (cf. Griffin et al. 1988; Stefanik & Latham 1992). Given the proximity of the Hyades and length of time the cluster has been observed, the two techniques provide continuous coverage of a large range of binaries from a separation of 0.02 AU (conversion of the measured 2 day period, assuming a system mass of 1.4 $M_{\odot}$ and a conversion factor of 1.26 between separation and semimajor axis) to a separation of 50 AU. Nearly all of the 162-star Hyades speckle sample has been observed spectroscopically, and 52 binaries have published periods, of which 16 are also resolved with speckle. Although the mass ratios are not known for most of the spectroscopic systems, the fact that all the closest speckle binaries were seen with spectroscopy suggests that the spectroscopic survey has a similar sensitivity. The few additional spectroscopic systems detected in the overlap range but not detected with speckle are near the limit of the speckle survey; consequently, orbital motion could easily explain why these binaries were not resolved (Patience et al. 1998). A large sample of Praesepe members has also been investigated with long-term spectroscopic surveys (Mermilliod & Mayor 1999; Abt & Willmarth 1999), and these results are also included in the analysis of the larger range of separations (details in Appendix C).

4.3.2. *Pre–Main-Sequence Stars*

The youngest comparison sample of stars is drawn from the many observations of T Tauri stars in the nearby star-forming regions—Taurus, Ophiuchus, Chamaeleon, Corona Australis, and Lupus. Since these star-forming regions are ~140 pc distant, the speckle and direct-imaging studies covering 0.″19 to 4.″15 share the same 26–581 AU projected separation range as the α Per and Praesepe observations. Over this separation range, the 2 Myr comparison sample consists of the 254 stars that have been observed by both speckle and direct-imaging surveys (Ghez et al. 1993, 1997a; Leinert et al. 1993; Simon et al. 1995; Köhler & Leinert 1998). As with the open clusters, additional surveys exist that are sensitive to binaries with separations outside 26 to 581 AU. Direct-imaging surveys sensitive to systems wider than 4″ augment the separation-range coverage (Ghez et al. 1997a; Leinert et al. 1993; Köhler & Leinert 1998)—the direct-imaging sample is almost as large, with 240 stars. For binaries with separations less than 25 AU, the data are drawn from the 69-star 5 m speckle sample (9–25 AU; Ghez et al. 1993), the 82-star (some overlap with 5 m speckle) lunar occultation sample (1–25 AU; Simon et al. 1995), and the 53-star spectroscopy sample (Mathieu, Walter, & Myers 1989). In addition to the similarity in the observed separation range, the 2 Myr sample also covers a mass range comparable to that of the cluster stars; although more difficult to determine, estimates of the masses range from ~0.2 to 2.5 $M_{\odot}$, with the nearly all the T Tauri targets above 0.5 $M_{\odot}$.

Because of the excess emission and uncertain ages associated with young stars, the ΔK-values measured for T Tauri binaries do not uniquely correspond to a mass ratio, making the mass ratio sensitivity level of T Tauri surveys more difficult to quantify. Based on the results of multiwavelength studies that do determine mass ratios (White 1999; Ghez, White, & Simon 1997b; Hartigan, Strom, & Strom 1994) and on the set of theoretical evolutionary models (Baraffe et al. 1998) favored by the

TABLE 7

PRAESEPE SINGLE STARS

Object	Telescope	Date	$\Delta K_{\rm lim}$ at 0.″15	$q_{\rm lim}$	No. Comp.	Notes[a]
A 70	IRTF	1999 Feb 15	3.14	0.44	0	
A 365	IRTF	1999 Feb 13	2.35	0.47	0	
A 609	IRTF	1999 Feb 15	3.4	0.41	0	
A 1196.....	IRTF	1999 Feb 14	0	1.00	0	
A 1480.....	IRTF	1999 Feb 14	3.73	0.35	0	
A 1501.....	IRTF	1999 Feb 13	1.87	0.54	0	
A 1528.....	IRTF	1999 Feb 13	2.78	0.41	0	
A 1583.....	IRTF	1999 Feb 13	2.32	0.48	0	
I 563.....	IRTF	1999 Feb 15	3.69	0.34	0	
II 490	IRTF	1999 Feb 14	4.39	0.23	0	
II 582	IRTF	1999 Feb 15	2.6	0.51	0	
JS 88	IRTF	1999 Feb 15	3.54	0.36	0	
JS 495.....	IRTF	1999 Feb 15	3.66	0.33	0	
JS 532.....	IRTF	1999 Feb 15	3.08	0.46	0	
JS 589.....	IRTF	1999 Feb 14	4.08	0.29	0	
JS 600.....	IRTF	1999 Feb 15	3.2	0.44	0	
KW 16	IRTF	1999 Feb 14	0	1.00	1	? (B91), S (M), B (MM99)
KW 38	IRTF	1999 Feb 14	0	1.00	0	S (M), S (P&W)
KW 40	IRTF	1999 Feb 13	2.6	0.42	2	S (M), S (P&W), B (B&C), T (AW99)
KW 45	Palomar	1996 Jan 9	4.16	0.30	0	S (M)
	IRTF	1998 Feb 18				
KW 47	IRTF	1999 Feb 14	4.58	0.21	1	B (MM99)
KW 50	Palomar	1996 Jan 9	4.25	0.25	0	S (M), B (AW99)
	IRTF	1998 Feb 18				
KW 100.....	Keck	1999 Jan 7	3.86	0.29	0	S (MM99)
KW 114.....	Palomar	1996 Jan 9	4.67	0.25	0	S (M), S (P&W)
	IRTF	1998 Feb 18				
KW 124.....	Palomar	1996 Jan 9	4.13	0.30	0	S (M), S (P&W)
	IRTF	1998 Feb 18				
KW 142.....	Palomar	1996 Jan 9	3.36	0.39	1	S (M), B (MM99)
	IRTF	1998 Feb 18				
KW 143.....	Palomar	1996 Jan 9	4.46	0.27	1	S (M), B (P&W) 0.″0441
	IRTF	1998 Feb 18				
KW 146.....	IRTF	1998 Feb 19	3.95	0.32	0	S (P&W)
KW 150.....	Palomar	1996 Jan 9	4.86	0.22	0	S (M), S (P&W), S (AW99)
	IRTF	1998 Feb 18				
KW 154.....	Palomar	1996 Jan 9	3.89	0.33	0	S (M), S (P&W)
	IRTF	1998 Feb 18				
KW 155.....	IRTF	1998 Feb 19	2.7	0.47	0	S (MM99)
KW 181.....	Keck	1999 Jan 7	3.2	0.43	1	B (MM99)
KW 182.....	IRTF	1999 Feb 15	4.39	0.23	1	S (B91), B (MM99)
KW 204.....	Palomar	1996 Jan 8	4.89	0.20	0	S (M), S (P&W), S (AW99)
	IRTF	1998 Feb 18				
KW 207.....	Palomar	1996 Jan 8	4.9	0.23	0	S (M), S (AW99)
	IRTF	1998 Feb 18				
KW 217.....	Keck	1999 Jan 6	4.53	0.20	0	S (B91), S (MM99)
KW 218.....	IRTF	1999 Feb 14	3.92	0.32	0	S (M), S (MM99)
KW 222.....	Keck	1999 Jan 6	4.89	0.16	0	S (MM99)
KW 226.....	Palomar	1996 Jan 9	3.36	0.38	0	S (M), S (P&W)
	IRTF	1998 Feb 19				
KW 227.....	IRTF	1998 Feb 18	2.39	0.52	0	S (B91), S (MM99)
KW 229.....	Palomar	1996 Jan 9	3.89	0.29	0	S (M), B (AW99)
	IRTF	1998 Feb 18				
KW 238.....	Keck	1999 Jan 7	3.14	0.44	0	S (MM99)
KW 239.....	IRTF	1998 Feb 20	3.49	0.40	0	S (MM99)
KW 244.....	IRTF	1999 Feb 14	4.48	0.22	1	B (B91) 0.4 days
KW 253.....	Palomar	1995 Nov 13	3.54	Giant	0	S (B91), S (M), S (AW99)
KW 258.....	IRTF	1999 Feb 15	3.58	0.36	0	
KW 265.....	Palomar	1995 Nov 12	3.73	0.29	1	B (M) 0.″425, S (P&W), S (B&C), S (AW99)
	IRTF	1998 Feb 19				
KW 268.....	IRTF	1998 Feb 18	1.87	0.60	1	B (MM99)
KW 271.....	IRTF	1998 Feb 18	2.39	0.49	0	S (M)

TABLE 7—*Continued*

Object	Telescope	Date	$\Delta K_{\rm lim}$ at 0.″15	$q_{\rm lim}$	No. Comp.	Notes[a]
KW 276.....	Palomar	1995 Nov 12	3.8	0.31	1	S (M), S (P&W), B (B&C), S (AW99)
	IRTF	1998 Feb 18				
KW 279.....	Palomar	1995 Nov 12	2.49	0.43	1	S (M), S (P&W), B (B&C), B (AW99)
	IRTF	1998 Feb 18				
KW 283.....	Palomar	1995 Nov 12	2.7	Giant	0	S (B91), S (M), S (P&W), S (AW99)
KW 286.....	Palomar	1996 Jan 9	4.13	0.30	0	S (M), S (P&W), S (B&C)
	IRTF	1998 Feb 19				
KW 292.....	Palomar	1996 Jan 9				
	IRTF	1998 Feb 19	4.08	0.30	1	B (B91), S (M)
KW 293.....	IRTF	1999 Feb 15	3.49	0.38	0	S (MM99)
KW 295.....	IRTF	1998 Feb 18	2.6	0.48	0	
KW 300.....	Palomar	1995 Nov 13	3.45	0.28	1	S (M), S (P&W), B (B&C), B (AW99)
	IRTF	1998 Feb 18				
KW 318.....	Palomar	1996 Jan 8	5.05	0.19	0	S (M)
KW 323.....	Palomar	1996 Jan 8	4.6	0.25	0	S (M)
KW 328.....	Palomar	1996 Jan 8	5.07	0.20	0	S (M), S (P&W), S (AW99)
	IRTF	1998 Feb 19				
KW 332.....	IRTF	1998 Feb 19	1.85	0.60	0	S (MM99)
KW 340.....	Palomar	1996 Jan 8	4.57	0.25	0	S (M)
KW 341.....	Keck	1999 Jan 6	4.74	0.18	1	B (MM99)
KW 348.....	Palomar	1996 Jan 9	3.58	0.29	0	S (M), S (P&W), S (AW99)
	IRTF	1998 Feb 19				
KW 350.....	IRTF	1998 Feb 18	2.87	0.43	1	S (M), B (B&C)
KW 370.....	Palomar	1996 Jan 8	5.16	0.17	0	S (M), S (P&W)
KW 371.....	Palomar	1996 Jan 8	4.57	0.20	1	B (MM99)
KW 375.....	Palomar	1996 Jan 8	5.11	0.19	0	S (M), S (P&W)
	IRTF	1998 Feb 20				
KW 396.....	IRTF	1999 Feb 15	3.76	0.33	0	S (MM99)
KW 411.....	IRTF	1998 Feb 19	2.6	0.48	0	S (M), S (MM99)
KW 416.....	IRTF	1998 Feb 19	1.89	0.58	1	B (MM99)
KW 418.....	Keck	1999 Jan 7	3.49	0.35	0	S (MM99)
KW 421.....	Keck	1999 Jan 6	4.57	0.20	0	S (MM99)
KW 429.....	Palomar	1996 Jan 9	4.01	0.32	0	S (M)
	IRTF	1998 Feb 20				
KW 439.....	IRTF	1999 Feb 14	4.89	0.18	0	S (M), B (MM99)
KW 445.....	Palomar	1996 Jan 9	4.25	0.28	0	S (M), S (P&W)
	IRTF	1998 Feb 20				
KW 449.....	IRTF	1999 Feb 13	2.5	0.43	0	S (M)
KW 454.....	Keck	1999 Jan 6	3.69	0.34	0	S (B91), S (MM99)
KW 459.....	Palomar	1996 Jan 9	4.11	0.30	0	S (M)
KW 472.....	IRTF	1998 Feb 20	1.83	0.61	0	
KW 478.....	IRTF	1999 Feb 15	2.78	0.48	0	
KW 496.....	IRTF	1999 Feb 14	3.98	0.32	1	S (B91), B (MM99)
KW 515.....	IRTF	1999 Feb 15	3.4	0.39	1	? (B91)
KW 534.....	IRTF	1999 Feb 13	3.2	0.36	1	S (M), S (P&W), S (B&C), B (AW99)
KW 536.....	IRTF	1999 Feb 14	4.06	0.31	0	S (M)
KW 538.....	IRTF	1999 Feb 13	2.87	0.43	0	S (M)
KW 549.....	IRTF	1999 Feb 15	4.46	0.21	0	
KW 553.....	Keck	1999 Jan 6	2.6	0.52	0	Nonmember

[a] Single (S), binary (B), or triple (T), and separation or period: (B91) Bolte 1991; (M) Mason et al. 1993; (MM99) Mermilliod & Mayor 1999; (P&W) Peterson & White 1984; (B&C) Burkhart & Coupry 1989; (AW99) Abt & Willmarth 1999.

analysis of the coevality of the GG Tau system (White et al. 1999), a mass ratio of $q = 0.25$ (similar to the $\Delta K = 4.0$ limit of the older samples) is roughly consistent with a cutoff of $\Delta K \sim 3$ for the younger T Tauri stars. In the 26–581 AU range, there are 76 binaries with ΔK of 3.0 or less. An additional 19 binaries satisfy the ΔK cutoff at wider separations extending to 1582 AU (11.″3), while there are 20 binaries in the 1–25 AU range and five spectroscopic systems with separations from 0.02 to 1 AU (periods from ~2 days to ~1 yr).

Another group of young stars that would provide interesting comparison samples is the population of young stars in Orion; current surveys, however, overlap only a limited portion of the 26–581 AU range considered for the clusters. Although the higher stellar densities associated with giant molecular clouds (GMCs) make these regions more likely progenitors of open clusters, the greater distance to the nearest GMC, Orion ($D \sim 450$ pc; Genzel & Stutzki 1989), prevents a complete comparison with the current survey. The results from several

large surveys—an optical *HST* survey (Prosser et al. 1994) in filters F547M ($\lambda_0 = 5446$ Å) and F875M and two *K*-band ground-based surveys (Simon, Close, & Beck 1999; Petr et al. 1998)—are included in the analysis of the binary separation distribution; the Orion data are compared with the wider cluster systems. The Wide-Field/Planetary Camera study of the Trapezium (Prosser et al. 1994) observed 319 targets in the Trapezium, the Simon et al. program covered 292 stars, and the Petr et al. data set includes 45 targets. The Orion samples have considerable overlap, however, and the total number of targets observed by at least one study is 480. Because the data are incomplete in both separation range and sensitivity, no attempt was made to correct the observed values so that they match the detection limits of the cluster surveys. Although the proportion of binaries measured by a study of wide (1000–5000 AU) common proper motion Orion systems (Scally, Clarke, & McCaughrean 1999) cannot be directly compared, the conclusions of the wide-binary search are discussed in § 5.3.

4.3.3. *Field Stars*

The oldest sample is the comprehensive spectroscopic and direct-imaging survey of 164 solar-neighborhood stars with spectral types ranging from F7 to G9 (mass range 0.85–1.3 $M_\odot$) (Duquennoy & Mayor 1991). The 26–581 AU range corresponds to 4.76–6.79 in the log (period [days]) units used in the G dwarf study; this conversion assumes that binaries have an average total mass of 1.4 $M_\odot$ (measured by the G dwarf survey) and that the semimajor axis is 1.26 times the projected separation (Fischer & Marcy 1992). This G dwarf survey lists both detected and corrected companion-star fractions; the corrected value accounts for undetected fainter companions down to the bottom of the main sequence. Since the corrected values correspond to a mass ratio detection limit of 0.10, the G dwarf results are reduced by 16% in order to restrict the correction to systems with $q > 0.2$, comparable to the cluster limits. The scale factor is based on the G dwarf mass ratio distribution (Duquennoy & Mayor 1991, their Fig. 8 and last line of their Table 7); 16% of the companions have mass ratios undetectable by the α Per and Praesepe cluster surveys.

Similar in age to the nearby G dwarfs but spanning a range in spectral type from A to M, the 106 northern stars within 8 pc provide another comparison sample. Drawing from many sources that enumerate the multiple systems in this well-surveyed sample, the binary census is estimated to be almost complete for all separations and for companion masses extending to the hydrogen-burning limit (Reid & Gizis 1997). With the large number of low-mass M stars in this sample, the uniform companion mass limit of 0.08 $M_\odot$ translates into a mass ratio limit above 0.25 for the ~40% of the sample with masses below 0.35 $M_\odot$. Because of the more similar mass range and sensitivity level, the G dwarf sample is a better comparison for investigations of the age dependence of the overall binary distribution and of the 26–581 AU companion-star fraction; however, the 8 pc sample does provide a data set with which the mass range can be extended.

5. DISCUSSION OF THE COMPANION-STAR FRACTION

5.1. *Definitions*

The multiplicity of each cluster can be determined by counting either the number of multiple systems or the number of companions. The multiple-star fraction compares the number of binaries (b) and triples (t) with the total sample consisting of singles (s), binaries, and triples:

$$\mathrm{MSF} = (b + t)/(s + b + t) ,$$

while the companion-star fraction counts the number of companions relative to the sample size:

$$\mathrm{CSF} = (b + 2t)/(s + b + t) .$$

The analysis presented in this discussion uses the CSF rather than the MSF. The calculation of the cluster CSF proceeds in two ways: as a single value over the restricted projected separation range of 26 to 581 AU (§ 5.2) and as a distribution function over a large range of projected separations (§ 5.3).

5.2. *CSF over the* 26–581 AU *Range*

Over the projected separation range of 26 to 581 AU, the multiplicity of the open clusters α Per, Praesepe, and the Pleiades is well determined for ΔK less than 4.0, or mass ratios $\lesssim$0.25 (see §§ 4.2 and 4.3). Based on the binary star detections within these projected separation and mass ratio boundaries, the α Per $\mathrm{CSF}_{26\text{–}581\ \mathrm{AU}}$ is 0.09 ± 0.03, the Praesepe $\mathrm{CSF}_{26\text{–}581\ \mathrm{AU}}$ is 0.10 ± 0.03, and the Pleiades $\mathrm{CSF}_{26\text{–}581\ \mathrm{AU}}$ is 0.12 ± 0.03. There appears to be no signifi-

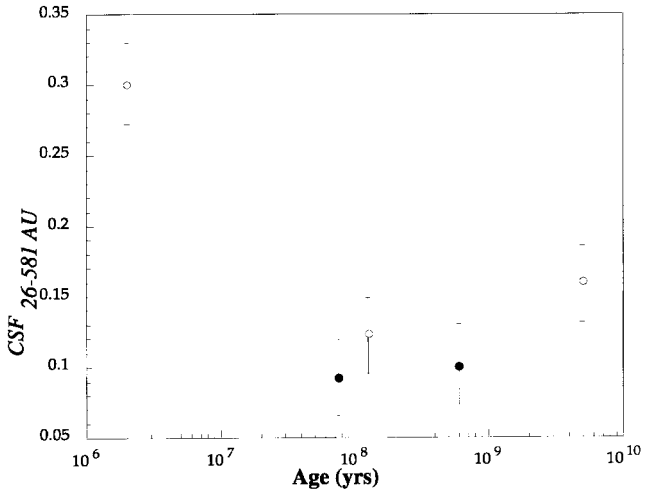

FIG. 2.—Age dependence of $\mathrm{CSF}_{26\text{–}581\ \mathrm{AU}}$. The CSF over the separation range 26–581 AU is plotted as a function of age for the two samples surveyed for this study and for three comparison samples; values from this work are noted by filled circles (α Per at 90 Myr and Praesepe at 660 Myr), while open circles mark the values from previous surveys (nearby T Tauri stars at 2 Myr, the Pleiades at 125 Myr, and field G dwarfs at 5 Gyr). Since the α Per and Praesepe data are sensitive to companions with $\Delta K < 4$ mag, the data from the comparison surveys are trimmed to this sensitivity level before calculating the CSF; details of this procedure are given in § 4.3. The result from the Hyades speckle survey is not included, because the separation-range coverage is different and the age is the same as that of Praesepe. All the samples older than the T Tauri stars have consistent, significantly lower, multiplicities than the T Tauri stars, suggesting that the CSF does not decline with age on timescales measurable with the cluster data.

cant difference between the $CSF_{26-581\ AU}$ values of the three clusters. The combined results from the 385 members of these three clusters yield a $CSF_{26-581\ AU}$ of 0.10 ± 0.02

Figure 2 plots $CSF_{26-581\ AU}$ as a function of age for the $q \gtrsim 0.25$ range for five different samples. Since both the solar-neighborhood G dwarf survey and the surveys of the nearby ($\sim$140 pc) star-forming regions of Taurus, Ophiuchus, Chamaeleon, Corona Australis, and Lupus cover the entire 26–581 AU range, these two age groups are easily compared with the three clusters α Per, the Pleiades, and Praesepe. The criteria used to construct the comparison samples are discussed in § 4.3.2, and the resulting CSF for the T Tauri stars is 0.30 ± 0.03 and is 0.16 ± 0.03 for the G dwarfs. Both α Per and Praesepe have CSFs 3 times lower than the T Tauri stars (Ghez et al. 1993, 1997a; Leinert et al. 1993; Simon et al. 1995; Köhler & Leinert 1998) but comparable to the older solar-neighborhood G dwarfs (Duquennoy & Mayor 1991).

One proposed explanation of the factor of 2 discrepancy between the CSF of pre–main-sequence stars and solar-aged stars is the disruption of multiple systems over time (cf. Ghez et al. 1993). Theoretical *N*-body models by Kroupa (1995a, 1995b) of clusters with an initial total CSF (over all separations) of 1.0 predict different trends in total multiplicity depending upon the initial stellar density, and these trends can be compared with the observational results. Although the evolutionary models predict the most pronounced effect on the binary fraction within the central 2 pc of a cluster, they also suggest that the overall binary fraction changes with age (Kroupa 1995a). Four cases are considered for the theoretical models: a loose association of binaries comparable to Taurus, a dense region comparable to the Trapezium, and two models with intermediate stellar densities. The typical separation between cluster members in the Hyades of 0.02 pc (M. Simon 1997, private communication) is intermediate between the mean separation of 0.003 pc for the Trapezium (McCaughrean & Stauffer 1994) and the wide spacing of 0.3 pc (Gómez et al. 1993) for Taurus members. The theoretical models predict that the binary fraction of a loose population declines by 10% to 25% from 2 Myr to the age of α Per and then falls by an additional $\sim$10% over the age range of the clusters, while the dense populations experience a rapid drop in binary fraction of 60% to 70% before the age of even the youngest star-forming regions and then remain at a constant low value. For the two intermediate densities more representative of the open clusters, the CSF evolution over the $\sim$600 Myr covered by the clusters also declines by at most $\sim$10%. Under the assumption that the CSF evolution for the restricted separation range observed follows the same evolutionary trend as the total CSF, the cluster portion of Figure 2 can be compared with these simulations; since the T Tauri star sample is from a lower stellar density region, it cannot be included in the examination of evolution. Although the lack of change in the cluster CSF is consistent with the simulations, the predicted effect of $\sim$1% (10% of the cluster CSF) is within the uncertainty, limiting the significance of this test. Studies of younger samples with similar densities are required for a more conclusive exploration of evolution as a possible cause of the observed CSF differences. Alternatively, the high CSF of the nearby dark cloud star-forming regions may be a consequence of different environmental conditions such as stellar density (Kroupa 1995a, 1995b) or temperature (Durisen & Sterzik 1994).

Although previous results from the Hyades speckle survey covering a closer, narrower separation range of 5 to 50 AU were consistent with a decline in the CSF with age (Patience et al. 1998), the current data sets—which cover a different, wider separation range and provide more data points—do not support a systematic reduction in the CSF with age that occurs on timescales longer than a few times 10^7 yr. Another study (Mason et al. 1998) that suggested a tentative decline in multiplicity with age also focused on a closer separation range—2 to 127 AU—than the current α Per and Praesepe surveys. The difference in conclusion between surveys probing different separation ranges suggests that examining the CSF over a wider range is important. The overall CSF distribution plotted in Figure 4*a* and discussed in the next section may explain the discrepant Hyades result.

5.3. *Overall CSF Distributions*

An assessment of the total CSF for open clusters covering all separations $\leq$581 AU and all magnitude differences $\Delta K < 4$ (mass ratios $\gtrsim$0.25) is estimated by combining the 26–581 AU results from the three cluster surveys described above with spectroscopic surveys of the Hyades and Praesepe and with a speckle imaging survey of the Hyades that extends the data to closer separations (see § 4.3.1). Merging the results assumes that all four clusters exhibit the same distribution, but this is supported by both the 26–581 AU speckle/AO data for three of the clusters and the 0.05–3 AU spectroscopic data for the Hyades and Praesepe. A series of Kolmogorov-Smirnov (K-S) tests comparing the imaging portion of each pair of clusters over their common separation range shows no significant difference between any pair; Figures 3*a*–3*d* show the α Per, Praesepe, Pleiades, and Hyades distributions individually. The combined cluster CSF, plotted in Figure 4*a*, extends over 4.5 decades of separation (0.02–581 AU). Summing the CSF in each bin over the entire range produces a total observed CSF for the clusters of 0.48 ± 0.05. Based on a Gaussian fit to the data, also shown in Figure 4*a*, the peak of the binary distribution occurs at a value of log (sep. [AU]) $= 0.6 \pm 0.1$ ($4^{+1}_{-1.5}$ AU).

The CSF distributions of younger and older samples, constructed from the surveys described in § 4.3, are shown in Figures 4*b*–4*d*. The oldest sample is the solar-neighborhood ($\leq$22 pc) G dwarf survey, which covers a range larger than the entire separation range of the cluster distribution. Figure 4*b* shows the G dwarf distribution, including the incompleteness corrections applied to the entire sample. Over the same 0.02–581 AU range covered by the cluster distribution, the corrected G dwarf CSF is 0.49 ± 0.05; reducing this value by 16% to 0.41 ± 0.05 provides the best estimate to account for differences in companion detection sensitivity (see § 4.3.3). Modeled as a Gaussian, the distribution has a peak at log (sep.) $= 1.6 \pm 0.2$ (40^{+23}_{-15} AU), significantly different from the cluster value. The shifted cluster peak relative to the G dwarf distribution explains why the Hyades CSF measured over the 5–50 AU range was larger than the G dwarf value while the CSF observed in the 26–581 AU range is consistent with the solar-neighborhood value.

Figure 4*c* shows the distribution for nearby T Tauri binaries with $\Delta K \leq 3$ ($q \gtrsim 0.25$) in Taurus, Ophiuchus, Chamaeleon, Corona Australis, and Lupus. Compared with the cluster CSF histogram, the overall T Tauri CSF distri-

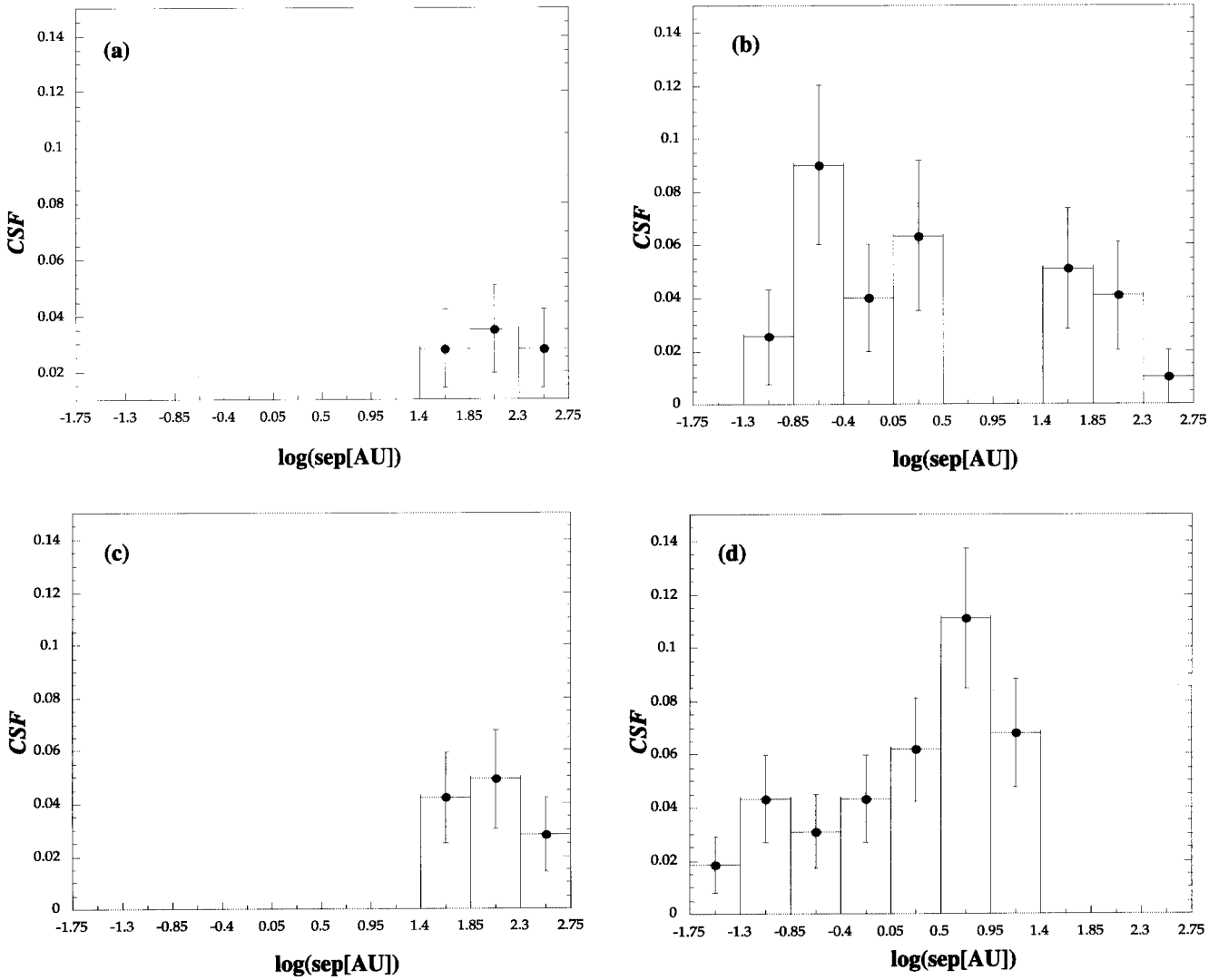

FIG. 3.—CSF distributions of the open cluster samples. Individual CSF distributions for each of the four open clusters are plotted over the range of separations covered by large-scale multiplicity surveys. The data for (*a*) the α Per distribution are taken from the current survey, while (*b*) the Praesepe plot includes spectroscopic binaries in addition to the speckle systems reported in the current survey. The comparison samples of (*c*) the Pleiades and (*d*) the Hyades are also shown; the Pleiades binaries were detected by an AO survey, and the Hyades represent a combination of spectroscopic and speckle systems. The references for the cluster surveys are given in §§ 2 and 4.3.1, and Table A1 lists the specific binaries that are included in each bin of the distributions.

bution has a larger integrated value and the peak is located at larger separations; for the same 0.02–581 AU range as the cluster distribution, the observed CSF is 0.69 ± 0.08. A Gaussian fit to the nearby T Tauri data yields a peak location of log (sep.) $= 1.8 \pm 0.2$ (62^{+38}_{-22} AU), which is consistent with the G dwarf peak but more than 3 σ larger than the cluster value of 4 AU. Another set of young binaries, drawn from optical *HST* images of Orion (Prosser et al. 1994) and speckle/AO IR images of the Trapezium region (Petr et al. 1998; Simon et al. 1999), are plotted in Figure 4*d*. Since these data sets are limited in their separation-range coverage, a Gaussian is not fitted to the Orion data. Incompleteness limits the ability to determine whether the distributions are different.

Brandner & Köhler (1998) have suggested that the field G dwarf binary distribution represents a superposition of contributions from different populations, although they did not estimate the relative contributions. Figure 5 compares the fits with the separation distributions of the T Tauri (*dotted line*), open cluster (*thin solid line*), and field (*dashed line*) samples. Since the G dwarf data have been corrected to account for companions down to the bottom of the main sequence, the Gaussian fitted to the field has been scaled down (by the same factor of 0.84 explained in § 4.3.3) so that the sensitivity is comparable to the cluster and T Tauri distributions. Taking the cluster distribution as representative of stars forming in giant molecular clouds,[3] the best fit to the G dwarf distribution is obtained for a combination of 30^{+15}_{-10}% dark cloud binaries and 70^{+10}_{-15}% GMC binaries. The best fit is determined by minimizing the χ^2 difference between the Gaussian fits to the scaled G dwarf distribution

[3] The cluster distribution is intended to represent the shape for a dense star-forming region, and this analysis is not meant to imply that such a large percentage of stars are members of open clusters at an earlier stage; the population of open clusters is not high enough to account for more than ~10% of all stars (Miller & Scalo 1978; Adams & Myers 2001).

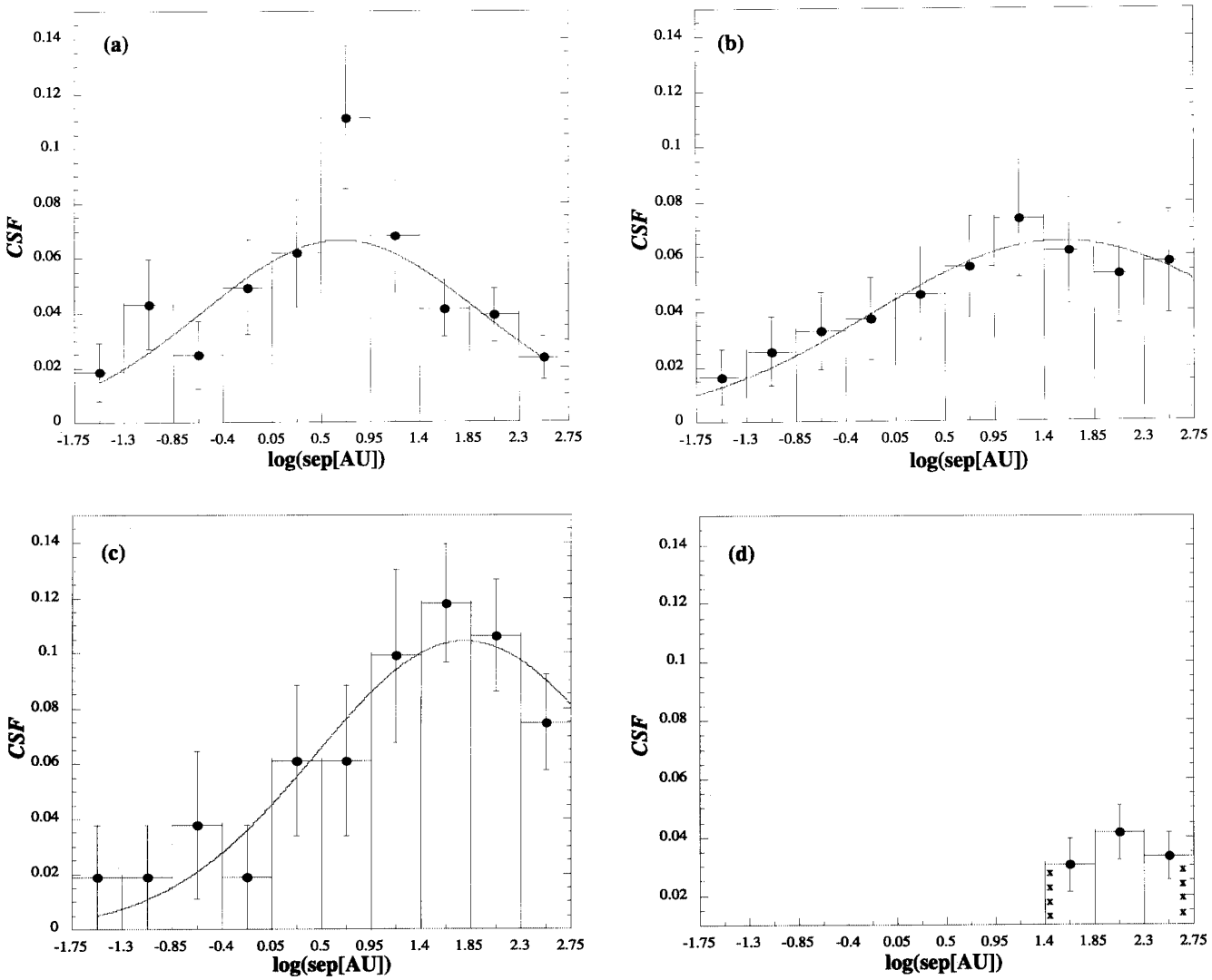

FIG. 4.—CSF distributions of four samples. Comprehensive CSF distributions spanning several orders of magnitude in separation are constructed for (*a*) cluster stars, (*b*) nearby G dwarfs, and (*c*) T Tauri stars. The less complete data available for Orion are also shown in (*d*); the crosses denote that the surveys are incomplete at the extremes of the bins. Compared with the original plot (Duquennoy & Mayor 1991) of the G dwarf distribution in terms of log (*P* [days]), each of the 0.45 log (sep. [AU]) bins is 0.675 in log *P*. The specifics of the G dwarf rescaling are given in § 4.3, which also describes the selection criteria for the T Tauri binary sample. The peak of the cluster distribution occurs at log (sep.) = 0.6 ± 0.1 ($4^{+1}_{-1.5}$ AU), which is a significantly smaller value than the location of the G dwarf peak value log (sep.) = 1.6 ± 0.2 (40^{+23}_{-15} AU) and the T Tauri distribution peak of log (sep.) = 1.8 ± 0.2 (62^{+38}_{-22} AU); the peak positions of the youngest and oldest samples are consistent with each other. Gaussian curve fits are included for the first three distributions; however, there are too few data for a fit to Orion.

and the cluster–T Tauri combination, with the differences measured at increments of 0.25 in log (sep.); the uncertainty represents the change in percentage that increases χ^2 by 1. In Figure 5, the thick solid line shows the best-fit superposition of T Tauri and cluster binaries.

This analysis implies that a significant fraction of field binaries (and by extension, all field stars) may have formed in lower stellar density regions such as Taurus, rather than in the denser and more populous GMC complexes that are the likely progenitors of open clusters. Although based only on the nondetection of wide proper-motion systems, Scally et al. (1999) reach a similar conclusion from their observations of the Orion Nebula cluster. The wide-binary analysis suggests an 80%–20% division between formation in a clustered environment and loose association. In contrast, star-count studies have proposed estimates as high as 96% of stars being formed in a clustered environment (not necessarily bound) rather than in a uniform distribution (e.g., Lada et al. 1991).

6. DISCUSSION OF OBSERVATIONAL TESTS OF BINARY FORMATION MODELS

The binary star properties measured by this survey provide observational tests of several binary formation models. The mass ratio ($q = M_{\rm sec}/M_{\rm prim}$) distribution (§ 6.1), the mass dependence of both the CSF (§ 6.3.2) and the *q*-distribution (§ 6.3.1), and the separation dependence of the *q*-distribution (§ 6.2) are all important observational constraints on formation mechanisms. Although not all theoretical simulations extend to a point in binary evolution at which main-sequence properties are determined, several formation scenarios, including capture (§ 6.4.1; McDonald & Clarke 1993, 1995; Sterzik & Durisen 1998) and fragmentation

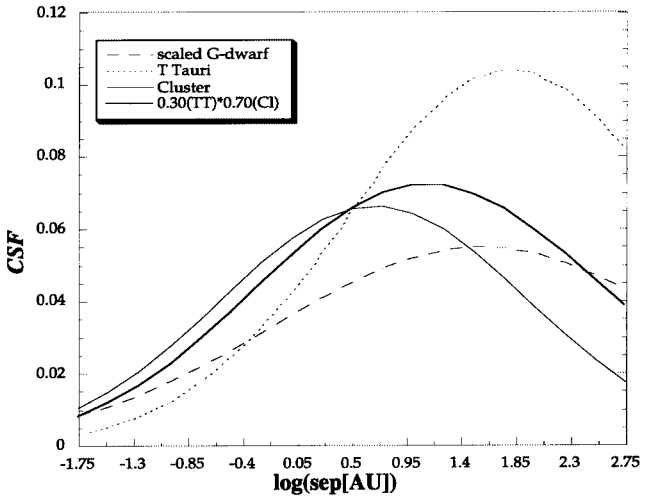

FIG. 5.—Gaussian fits to the CSF distributions. The fits to the scaled G dwarf sample (*dashed line*), T Tauri data (*dotted line*), and Hyades/α Per/Praesepe/Pleiades cluster sample (*thin solid line*) are plotted along with the combination of cluster and T Tauri distributions that best matches the shape of the G dwarf curve (*thick solid line*). Based on this very simple population synthesis, the data suggest that the G dwarf binary population is a combination of approximately one-third binaries formed in loose T associations and two-thirds binaries formed in higher stellar density regions.

(§ 6.4.2; Clarke 1996b; Bate & Bonnell 1997; Bate 2000, 2001), make specific predictions that can be compared with the open cluster data. The survey results are presented first along with comparisons with previous observations, and a discussion of the predictions from theoretical models follows.

6.1. *Mass Ratio Distribution*

The shape of the mass ratio (q) distribution presents a means of testing the predictions of capture theories, while the number of peaks in the q-distribution may provide an indication of the number of binary star formation mechanisms. The q-distributions for α Per, Praesepe, and the Pleiades over 26 to 581 AU and the Hyades over 5 to 50 AU all rise monotonically toward smaller mass ratios. Based on a series of K-S tests comparing each pair of these four clusters, none of the q-distributions are significantly different. Consequently, all the results are used to construct an overall cluster q-distribution, shown in Figure 6. This q-distribution consists of the 54 cluster binaries with mass ratios of 0.40 or greater; this limit was chosen so that incompleteness should not be a problem (see § 4.2). The histogram rises slightly toward systems with a smaller mass companion relative to the primary mass (low q), but it is also consistent with a flat distribution. Since there is no evidence for bimodality in the cluster data, the q-distribution does not support the idea of binary formation by two processes with distinctly different mass ratio distributions. Comparisons with particular models are made in § 6.4.

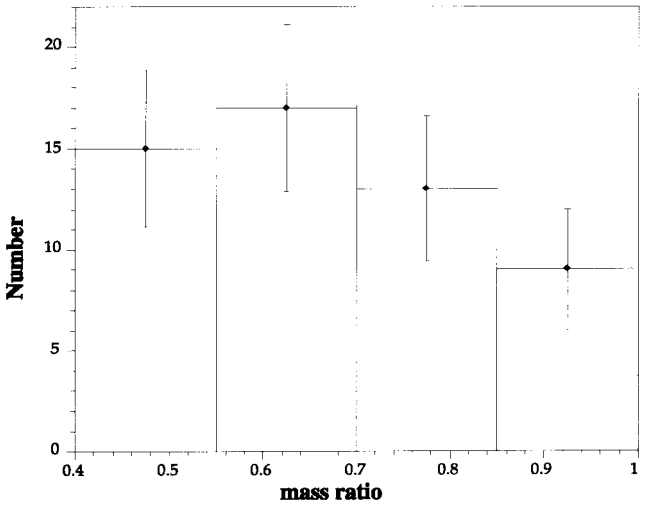

FIG. 6.—Cluster q-distribution. The mass ratio distribution of the combined cluster sample is shown. In order to avoid any detection bias, the binaries only include systems with mass ratios of 0.40 or greater and with specific separations. For the Hyades, the separation range is restricted to 5–50 AU, while the range considered for α Per, Praesepe, and the Pleiades is 26–581 AU.

The slope of the q-distribution can be compared with the expectations of different types of capture models. The increase toward smaller mass ratios is not steep enough to be consistent with the $q^{-2.35}$ Salpeter power law. The more shallowly sloped function resulting from random pairing of two stars drawn from a mass function representative of an open cluster population is consistent with the observations; the mass function used for this simulation was a combination of three power laws: $N(m) \sim m^{1.5}$ for $m < 0.1$, $N(m) \sim m^{-1.05}$ for $m = 0.1$–1.0, and $N(m) \sim m^{-2(1+\log m)}$ for $m > 1.0$ (Reid & Gizis 1997; Meusinger, Schilbach, & Souchay 1996).

6.2. *Separation Dependence of the q-Distribution*

The combined open cluster data cover a large range of binary star separations (from 5 to 581 AU) and encompass the important size scale associated with circumstellar disks. Two formation scenarios—disk fragmentation and models of accretion following fragmentation—suggest that the binary properties should depend upon the system separation. Dividing the 54 cluster binaries with mass ratios exceeding 0.4 at successively larger binary separations and comparing the close and wide q-distributions does not reveal distinct mass ratio distributions. In particular, when the sample is split at larger separations comparable to the sizes associated with disks ($\sim$100 AU), the mass ratio distribution of the closer systems remains indistinguishable from that of the wider systems. A tentative break at $\sim$200 AU in the separation distribution of mass ratios is seen in studies of nearby T Tauri binaries (White & Ghez 2001; Köhler & Leinert 1998), but these T Tauri surveys extend to larger separations than the cluster observations, and the number of cluster binaries with separations over 200 AU is small. Previous results based on the comprehensive G dwarf survey (Mazeh et al. 1992) suggest that the q-distribution of the closest binaries with periods less than 3000 days, or separations less than 5 AU, is different from the longer period q-distribution, with a larger proportion of similar-mass systems; again the cluster data would not be expected to reproduce this result, since the dividing separation is at the boundary of the observed range.

6.3. *Mass Dependence of the CSF and q-Distribution*

With a total of 544 main-sequence stars ranging in spectral type from B to early M, or masses of $\sim$5 to 0.5 $M_\odot$, the

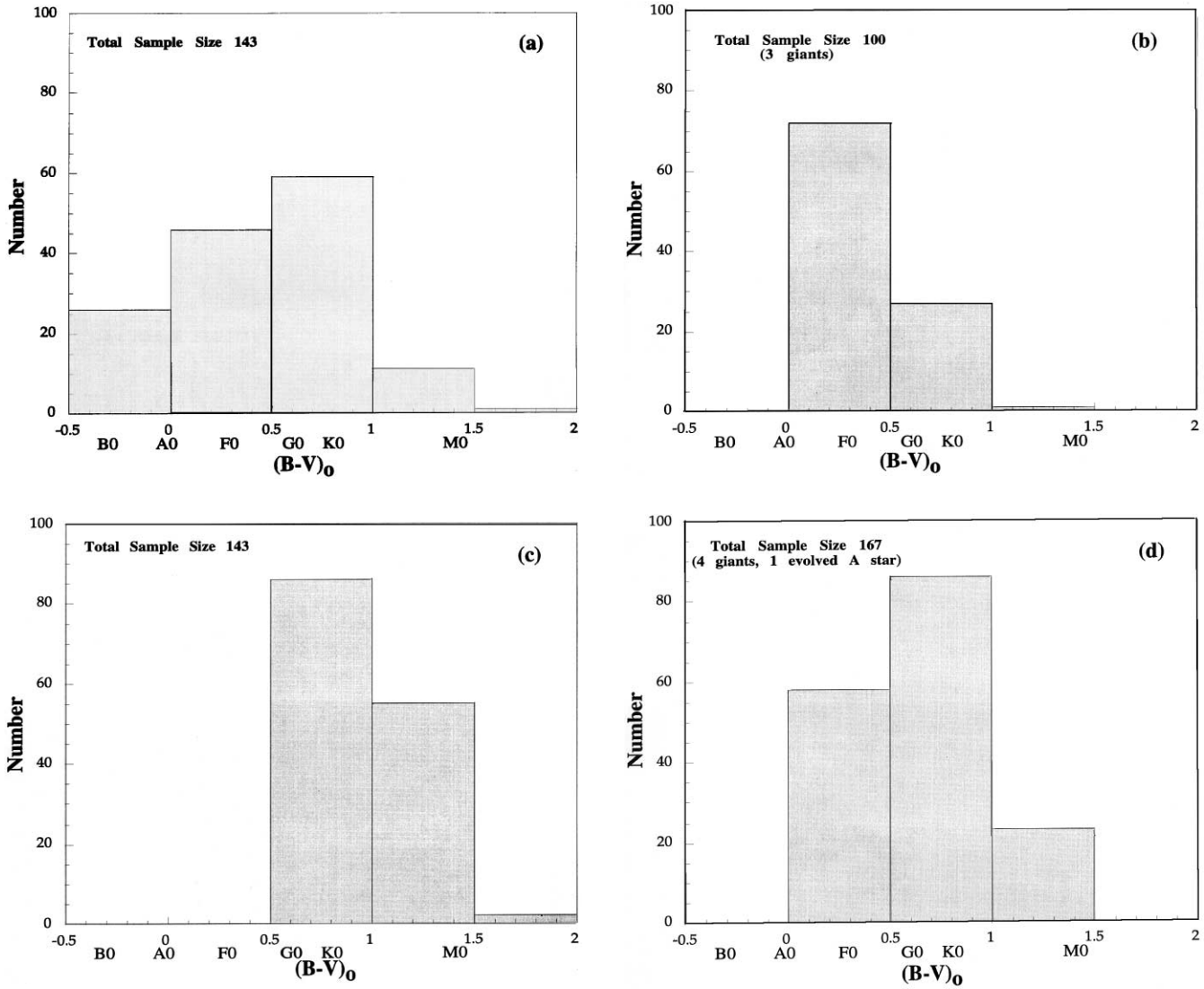

FIG. 7.—Cluster $(B-V)_0$ color histograms. Histograms of the $(B-V)_0$ color are displayed for the stars in the current surveys of (*a*) α Per and (*b*) Praesepe. Two comparison samples observed in previous high-resolution surveys and included in much of the analysis are also plotted: (*c*) the Pleiades and (*d*) the Hyades. Considering all four surveys, the spectral types observed cover B to early M, which corresponds to $(B-V)_0$ colors from -0.2 to 1.7 and masses between 5 and 0.5 $M_\odot$. The Praesepe sample is limited to early types, the α Per and Hyades samples include both early-type stars, and the Pleiades sample is composed almost exclusively of solar-type stars. The range of stellar masses observed is important for testing mass-dependent predictions of binary formation models.

combined cluster data set presents a unique sample to investigate possible correlations with binary mass. Among the 544 stars are 54 binaries with $q > 0.4$ and 63 binaries with $\Delta K < 4$ mag ($q \gtrsim 0.25$). Both capture and fragmentation models predict specific trends in the CSF and *q*-distribution, making the mass dependence of these properties an important discriminant between different formation scenarios. Only the youngest cluster, α Per, still contains the more massive, short-lived B stars. The three speckle surveys of α Per, Praesepe, and the Hyades include most of the A and F stars in these clusters. Since the AO Pleiades survey concentrated on solar-type stars, it contributes mainly G and K stars. Additional G and K stars are provided by the α Per and Hyades surveys. Finally, the Pleiades observations and the α Per *HST* data include a small sample of M stars. Figures 7*a*–7*d* plot spectral type/$(B-V)_0$ color histograms for each sample of stars in the four open clusters.

6.3.1. *Mass Ratio Distribution versus Mass*

The mass ratios of the 54 binaries used to construct the overall mass ratio distribution were sorted by their color and separated into two distributions; the dividing color was varied and K-S tests were performed to determine whether the two sets of mass ratios are significantly different. At a dividing color of $(B-V)_0 = 0.53$ (spectral type F8, mass $\sim$1.2 $M_\odot$), the two *q*-distributions are the most different and have only a 0.2% probability of being drawn from the same population. Figure 8 normalizes the *q*-distribution in each subsample by the number of binaries and compares the fraction of binaries as a function of *q* for the higher and lower mass primary stars. The *q*-distribution for higher mass primaries increases sharply toward smaller *q*-values, while the *q*-distribution of lower mass primaries is relatively flat. An extension of this trend of fewer small-*q* binaries for lower mass primaries is seen in the 8 pc sample, which consists

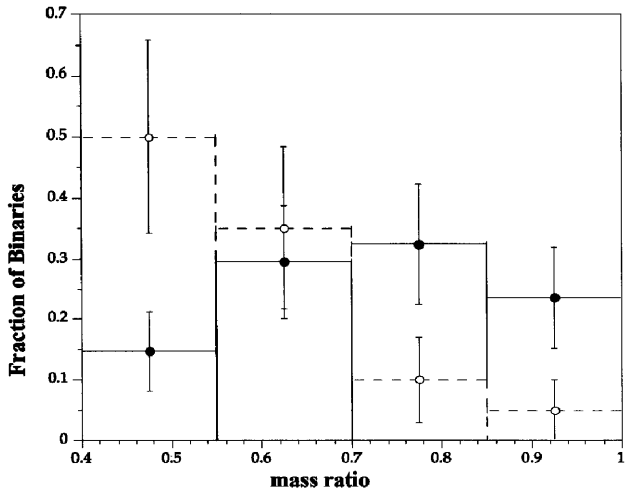

FIG. 8.—Mass dependence of the q-distribution. The normalized mass ratio distributions for bluer (higher mass) binaries (*dashed line*) and redder (lower mass) binaries (*solid line*) are plotted. At a dividing $(B-V)_0$ color of 0.5, which corresponds to a spectral type of ~F7, the distributions are significantly different, with the lower mass systems showing fewer low mass ratio companions. This deficit of low-mass companions occurs above the stellar limit.

largely of M stars; the q-distribution for the 8 pc sample increases toward $q \sim 1$ systems (Reid & Gizis 1997).

6.3.2. *CSF versus Mass*

In order to investigate the mass dependence of the CSF, the 544-star open cluster sample, covering masses from 0.5 to 5 $M_{\odot}$, is divided into four roughly equal subsets based on the dereddened target color. The binaries included in this analysis are the 63 cluster binaries with $\Delta K \leq 4$ mag and separations from 5 to 50 AU (for the Hyades) or 26 to 581 AU (for the more distant open clusters). Although the Hyades data cover a different separation range, the overall CSF is comparable to the farther clusters, and the Hyades stars constitute a similar fraction of each color group (~0.3). Figure 9 plots the CSF calculated for each of the four groups as a function of the median color of the subset; the straight line on the plot represents the CSF of the entire sample, 0.12 ± 0.01. The combined data show a higher CSF for the lower mass stars. The best-fit line through the combined data has a slope of 0.13 ± 0.04, which is 3 σ different from a flat line.

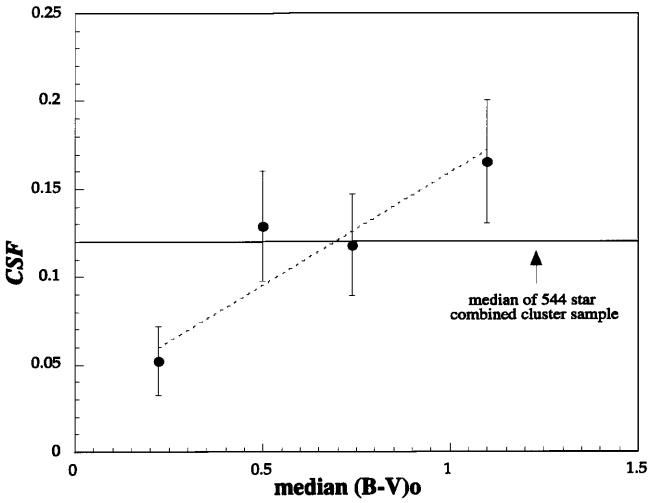

FIG. 9.—Mass dependence of the CSF. The CSF calculated for four ranges of target star color is plotted as a function of the median color; the 545-star sample is split into four subsets with ~136 stars in each color range. Only binaries with $\Delta K < 4$ mag and separations of 26–581 AU (for α Per, Praesepe, and the Pleiades) or 5–50 AU (for the Hyades) are included in the calculation. Since the mass ratio limit is comparable, the redder color bins have progressively lower companion mass limits. Over the range of stellar colors (masses) considered for this survey, the CSF rises toward redder colors or smaller masses. The upward slope of 0.13 ± 0.04 is 3 σ different from a flat line. An decrease in CSF with mass is inconsistent with both the diskless small-N capture and the scale-free fragmentation formation scenarios.

The upward trend in multiplicity with decreasing mass over the A–K star range was also suggested by previous results from the 8 pc sample (cf. Reid & Gizis 1997), but the open cluster sample contains many more early-type stars and extends to the B stars. Over a similar mass range to that of the cluster data set, a different trend of increased CSF for Herbig Ae/Be stars relative to T Tauri stars has been reported in an AO survey (Bouvier & Corporon 2001), but these results depend strongly upon the large incompleteness corrections applied to the Herbig Ae/Be data—the cluster data in Figure 9 are not corrected. This sample contains few M stars, and it is difficult to directly compare previous results involving lower mass M stars that extend below the masses considered for the cluster surveys, but several M star survey results are mentioned for completeness. The 8 pc M dwarf data are not included in Figure 9, because the low masses of these stars makes a $\Delta K = 4$ ($q \lesssim 0.25$) companion below the stellar limit, and detecting such faint objects is difficult. When measured differently with a companion mass cutoff rather than a mass ratio cutoff as in the open cluster results, a decline in total CSF (over all separations) between G dwarfs and M dwarfs has been reported (Fischer & Marcy 1992; Reid & Gizis 1997). Over the separation range 14 to 825 AU, a low fraction of binaries among Hyades M stars has also been observed (Reid & Gizis 1997). Preliminary results from a continuation of the field M dwarf survey show a similar M dwarf CSF to the G dwarf value (Udry et al. 2000), but this study only includes spectroscopic systems. With the discovery of an increasing sample of lower mass L dwarfs, the binary fraction of this population is beginning to be explored, and initial results suggest that, as with M dwarfs, the proportion of binaries is low (Reid et al. 2001). In conclusion, when measured over the late B to late K star range with a mass ratio limit, the CSF increases with decreasing mass; however, studies that measure or correct to a companion mass limit and extend to M stars show different trends of a CSF that is higher for Herbig Ae/Be than T Tauri pre–main-sequence stars and that declines over the G–M star range in the field.

TABLE 8A

SUMMARY OF OBSERVATIONS

Observable	Trend in Speckle/AO/*HST* Cluster Data
q-Distribution	Flat or slightly rising toward lower q
q vs. separation	No dependence
q-Distribution vs. mass	Steeper slope for higher mass
CSF vs. Mass	Lower for higher mass

6.3.3. *Summary of Observational Trends*

Several trends in the binary properties are evident from the sample of 544 open cluster members with spectral types from B to M, containing 54 $q > 0.4$ binaries and 63 $q \gtrsim 0.25$ binaries, and with separations from 5 to 50 AU (for the Hyades) or 26 to 581 AU (for the farther clusters); Table 8A summarizes the observations. Considering binaries with $\Delta K < 4.0$ ($q \gtrsim 0.25$), the CSF increases for increasing color (equivalently, decreasing mass), as shown in Figure 9. The mass ratio distribution from $q = 0.4$ to $q = 1.0$, given in Figure 6, is flat or slightly increasing toward smaller mass ratios. The mass ratio distribution has a different shape, however, depending upon the primary mass; the higher mass primaries exhibit a steeper rise toward smaller-q systems, as shown in Figure 8. Finally, there is no correlation with separation in the q-distribution over the 5–581 AU range covered by the cluster surveys.

6.4. *Comparison with Star Formation Models*

6.4.1. *Capture Models*

Capture occurring in small-N clusters generates binaries with sufficient efficiency to explain the observed total frequency of binary and multiple systems (see, e.g., McDonald & Clarke 1993, 1995; Sterzik & Durisen 1998). The first model of this class considered—small-N capture without disks (McDonald & Clarke 1993)—preferentially produces binaries composed of the two most massive stars, creating a distribution that increases toward unity, inconsistent with the observational data (Fig. 6). Because this type of capture preferentially forms binaries with the most massive stars, the resulting CSF is expected to decrease with decreasing primary mass, also contrary to the observed positive slope of the cluster data (Fig. 9). A further refinement of the small-N capture process includes the effects of circumstellar disks in the calculations. Disk-assisted capture randomizes the companion to the primary—again the most massive star—and creates more small-q binaries, similar to the observed distribution (Fig. 6; McDonald & Clarke 1995). Dynamical decay of few-body systems, another model of capture, predicts that the CSF is higher for more massive stars and that the q-distribution for more massive stars should have a steeper slope (Sterzik & Durisen 1998). Since the predicted trend in CSF as a function of mass involves a secondary-mass cutoff rather than a mass ratio limit, it is difficult to test this expectation with the limited dynamic range of the current survey. It is possible to compare the q-distributions in Figure 8 with the predicted effect of more small-q systems among the more massive primaries, and the observations match the theory. In summary, the observational data from the combined cluster sample are inconsistent with diskless small-N capture but consistent with disk-assisted small-N capture and dynamical decay of few-body systems. Table 8B lists the comparisons of observations with these capture models.

6.4.2. *Fragmentation Models*

The mass and separation dependences of the binary properties provide tests of several fragmentation models. One formation mechanism, disk fragmentation, is believed to operate over specific separation scales associated with the size of a circumstellar disk. The q-distribution does not show a significant difference for separations larger and smaller than a typical disk size (~100–200 AU), suggesting that disk fragmentation is not the predominant form of binary formation in this separation range. This conclusion, however, is limited by the separation range of the survey.

Another type of fragmentation—scale-free fragmentation—predicts that the properties of binaries should be independent of mass (Clarke 1996b). Specifically, the observed positive slope of the CSF versus mass (color) is a problem for this theory, which predicts that for data with a mass ratio cutoff, the CSF should be independent of mass. The expected straight line plotted in Figure 9 does not match the data. In addition, the observation that the q-distribution for higher mass stars is significantly different from that of the lower mass stars contradicts a scale-free formation process. Large-scale surveys that have measured a very low frequency of brown dwarf companions (e.g., Oppenheimer 1999; Macintosh et al. 2000) imply that the stellar limit (0.08 $M_{\odot}$) may be an important scale in the binary formation process, while the cluster results, which do not reach this limit, suggest that another, more massive scale may influence binary properties.

Numerical models of the fragmentation process cannot currently simulate the full evolution from molecular cloud core to observable binary properties; however, recent simulations of accretion onto protobinary fragments have generated several testable predictions. In an isolated environment, binaries that accrete more material from a rotating cloud core with high specific angular momentum are driven toward similar component masses: $q \sim 1$ systems (Bate 2000). Since the initial mass of the protobinary increases with separation (Bate 2000), close binaries need to accrete more material to obtain a given final mass; over a fixed separation range, more massive systems will also accrete more material. Both closer and more massive binaries should contain more $q \sim 1$ binaries based on these simulations. Since the close and wide distributions show no clear difference in the fraction of highest-q systems, the data do not show the predicted trend, but this may be due to the cutoffs in separation. The limited number of $q \sim 1$ systems also does not appear to vary with mass as expected. Accretion simulations modified to represent a clustered rather than a loose environment (Bate 2001) have a different outcome, since the stellar motion is not correlated with the gas, giving the infalling gas a low specific angular momentum. In this case, massive stars are expected to form more low-q binaries, in agreement with Figure 8.

It is also important to note that capture and fragmentation may not be separate processes, as fragmentation may produce the small clusters that are the initial conditions of the capture scenarios (see, e.g., Boss 1996). In summary, the observational trends are inconsistent with disk fragmentation, scale-free fragmentation, and simulations of accretion following fragmentation in a loose environment; a model of accretion following fragmentation in a cluster environment is consistent with the open cluster data. Table 8B summarizes the comparisons of observations and the fragmentation models.

7. DISCUSSION OF BINARY STAR EFFECTS ON STELLAR PROPERTIES

The presence of a companion star can both passively skew the measured stellar properties of the primary, if it is unresolved, and actively alter the distribution of gas and dust around forming stars. One interesting consequence of com-

TABLE 8B

SUMMARY OF COMPARISON WITH FORMATION MODELS

MODEL	q-DISTRIBUTION		q VS. SEPARATION		q-DISTRIBUTION VS. MASS		CSF VS. MASS	
	Prediction	Observed?	Prediction	Observed?	Prediction	Observed?	Prediction	Observed?
Small-N capture	Increase toward $q \sim 1$	No	...	...	...	...	Increase for higher mass	No
Small-N with disks	More lower-q	Yes	...	...	...	...	Increase for higher mass	?[a]
Few-body decay	...	...	...	...	Steeper for higher mass	Yes	Increase for higher mass	?[a]
Scale-free fragmentation	...	...	...	...	Independent of mass	No	Independent of mass	No
Disk fragmentation	...	...	Should show dependence	No[b]	...	...	...	...
Accretion in association	...	...	More $q \sim 1$ closer	No	More $q \sim 1$ for higher mass	No	...	...
Accretion in cluster	...	...	...	...	More low-q for higher mass	Yes	...	...

[a] Prediction for fixed companion mass limit, not mass ratio limit; data cannot address.

[b] May require larger separation range to properly test.

TABLE 9
X-Ray Detections and Binaries among Early-Type Stars

Sample	No. X-Ray Detections	No. Bin	$CSF_{X\text{-}ray}$	No. X-Ray Upper Limits	No. Bin[a]	$CSF_{no\ X\text{-}ray}$
Hyades	9	6	0.7 ± 0.3	14	5	0.4 ± 0.2
Praesepe	5	3	0.6 ± 0.3	27	7 (2)	0.19 ± 0.08
α Persei	8	4	0.5 ± 0.3	15	2	0.13 ± 0.09
Three clusters	22	13	0.6 ± 0.2	56	14 (2)	0.21 ± 0.06

[a] Numbers in parentheses indicate binaries with two early-type components.

panion stars is a possible explanation for the unexpected detection of X-ray emission from late B and A stars. Section § 7.1 investigates this effect. Section 7.2 discusses the role of companions in stellar rotational evolution.

7.1. *Binaries and X-Ray Emission from A Stars*

In order to investigate the role of lower mass companions in the X-ray detections of late B and A stars, this section considers a subsample of the cluster data set—the B and A stars in α Per, Praesepe, and the Hyades that have been targeted by both *ROSAT* and high-resolution multiplicity surveys. Since these stars lack the strong winds or dynamos that generate X-rays in O through early B and F through M stars (see Pallavicini 1989), unresolved companions may be the true source of the *ROSAT* detections. Binaries detected by speckle and spectroscopic surveys have separations within the error boxes, typically $\sim 10'' \times 10''$, of the *ROSAT* detections. Combining the results of the α Per, Praesepe, and Hyades surveys, a total of 90 stars in the $(B-V)_0$ color range of -0.13 to 0.30 have been searched for companions with speckle; half of these stars have also been included in spectroscopic multiplicity surveys (Abt 1965; Abt & Levy 1976; Bolte 1991; Burkhart & Coupry 1989, 1998; Prosser 1992; Morrell & Abt 1992; Stefanik & Latham 1992; Abt & Wilmarth 1999). Of these 90 stars, 78 were observed with either *ROSAT* raster scans or pointed observations, and 22 have X-ray detections (Randich et al. 1996; Prosser et al. 1996; Randich & Schmitt 1995; Stern, Schmitt, & Kahabka 1995). Table 9 lists the number of stars with X-ray detections or X-ray upper limits in each cluster and gives the number of binaries detected by either speckle or spectroscopy for each group.

All the speckle binaries have sufficiently small mass ratios for the companion to have a late enough spectral type to generate the observed X-rays. Some of the detected spectroscopic binaries, however, are SB2 systems consisting of two A stars, which would not explain the X-ray emission; the number of SB2's is listed in parentheses after the number of binaries in Table 9, and these binaries are not counted in the following CSF calculations. Most of the spectroscopic systems are SB1's, which have lower mass companions. The CSF of the subset with X-ray detections is $CSF_{X\text{-}ray} = 0.6 \pm 0.2$, and the corresponding value of the subset without X-ray detections is $CSF_{no\ X\text{-}ray} = 0.21 \pm 0.06$. Because of the limited dynamic range of the surveys, the $CSF_{X\text{-}ray}$ is not expected to be 1.0 even if each B6–A star has a companion producing the X-ray emission. For example, M star companions are not detectable. Although the faint-companion hypothesis was not the favored interpretation of a high-resolution study of Herbig Ae/Be stars—the younger counterparts to the cluster B and A stars—the Herbig Ae/Be results also reveal a larger number of binaries among stars having X-ray detections (six of 12) than among stars lacking X-ray emission (zero of 10) (Zinnecker & Preibisch 1994). This supports the cluster results of a $CSF_{X\text{-}ray} \sim 3$ times higher than the $CSF_{no\ X\text{-}ray}$, and both Herbig Ae/Be and cluster statistics suggest that companions may be responsible for the X-ray detections. Because of the small sample sizes, however, the cluster difference is only marginally significant; observations of a larger sample of early-type stars will be required to determine more conclusively whether low-mass companions can account for the apparent emission from late B to A-type stars.

7.2. *CSF and Stellar Rotation*

Since the solar-type stars [F7 and later, $(B-V)_0 = 0.50$; Kenyon & Hartmann 1995] in the youngest cluster, α Per, are in a unique stage of stellar rotational evolution characterized by a wide range of rotational velocities (Stauffer et al. 1985; Prosser 1992), the sample for the following analysis is limited to α Per members in this spectral range. Two competing theories involving binary stars have been proposed to explain the range of observed rotational velocities. As discussed in § 1, these models make opposing predictions for the CSF of slow and rapid rotators.

Among the 71 solar-type stars in α Per, the measured $v \sin i$ values cover the entire measurable range from over 200 km s^{-1} to less than 10 km s^{-1}. A division of the sample at a $v \sin i$ of 20 km s^{-1} places approximately equal numbers of targets in the slow and rapid categories, with 37 slow rotators and 34 rapid rotators. Over the projected separation range of 26 to 581 AU and $\Delta K < 4$ mag ($q \sim 0.25$–1.0), the CSF of the slow rotators is $CSF_{slow} = 0.19 \pm 0.07$ and the CSF of the rapid rotators is $CSF_{rapid} = 0.09 \pm 0.05$. The difference between the two values of multiplicity is not statistically significant ($\sim 1\ \sigma$), and changing the cutoff value for slow and rapid rotation does not alter the result.

Although the CSF does not vary with the stellar rotation rate over the complete range of separation and mass ratio, it is possible that only binaries with certain parameters such as close separations have a discernible effect on the primary star's rotation rate. Among the 10 solar-type binaries with separations from 26 to 581 AU and $\Delta K \leq 4.0$, there is no difference in the distribution of rotational velocities as a function of either mass ratio or separation. A similar result was found for the Pleiades (Bouvier et al. 1997). The Keck and Palomar observations in this α Per survey, however, are sensitive to separations closer than the 26–581 AU range used in the rest of this study. The sample of stars observed with higher resolution is small, but it is not biased toward either slow or rapid rotators, since the stars observed with

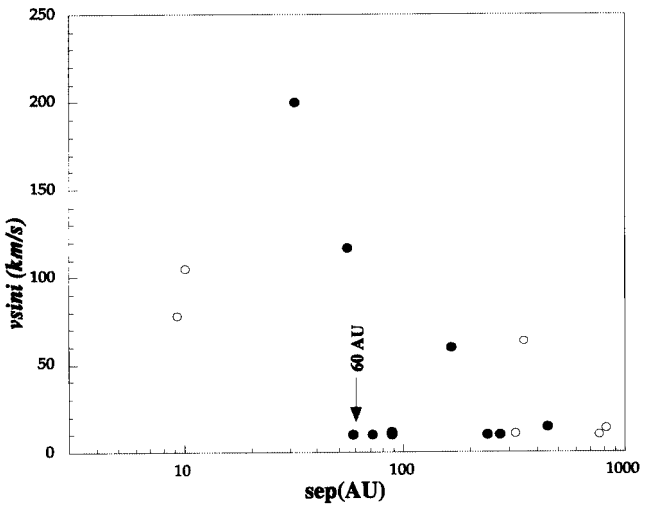

FIG. 10.—The α Per v sin i vs. separation. The rotational velocity is plotted as a function of binary separation for the solar-type stars in α Per. Since the largest rotational evolution occurs for solar-type stars, this sample is limited to binaries with spectral types later than F7, or colors of $0.50 \leq (B-V)_0 \leq 1.6$. Filled circles mark the binaries with separations of 26–581 AU and mass ratios exceeding 0.25. The open circles at small separations represent binaries separated by less than 26 AU that could only be detected with the higher resolving power of the Keck Telescope, while the open circles at larger separations represent binaries with small mass ratios (but with stellar companions) that could only be observed with the greater dynamic range of *HST*. Systems separated by less than 60 AU have significantly higher velocities than the wider pairs, suggesting that these stars lost their disk-braking mechanism earlier, possibly because of disk disruption by the companion star.

Keck and Palomar have a range of v sin i values comparable to that of the entire sample. The *HST* data are sensitive to wider and fainter systems than the 581 AU cutoff. Figure 10 plots the larger set of *all* 16 solar-type binaries detected in α Per and reveals a trend of increased rotational velocity with smaller separation. Dividing the sample of binaries at 60 AU results in a K-S test probability of only 2% that the close and wide systems have the same v sin i distribution. The median v sin i value is 105 ± 69 km s^{-1} for the binaries with separations less than 60 AU, but only 11 ± 21 km s^{-1} for the systems wider than 60 AU. Because of the small sample, this result is preliminary and needs to be confirmed. Among the binaries, separation rather than mass ratio appears to be a more important factor in determining stellar rotation rates. Assuming a connection between disk lifetime and rotation rate, the α Per results suggest that binaries with separations closer than 60 AU have shorter lived circumstellar disks that do not survive long enough to effectively slow the stellar rotation. The α Per result is consistent with the observation of reduced millimeter and submillimeter flux from T Tauri binaries with separations less than ~50–100 AU compared with wider binaries in several star-forming regions (Jensen, Mathieu, & Fuller 1994; Osterloh & Beckwith 1995; Jensen, Mathieu, & Fuller 1996).

8. SUMMARY

With near-infrared speckle and *HST* NICMOS images of α Per and Praesepe members, an accounting and analysis of the cluster binaries has been performed. Combining data from the IRTF, Palomar, Keck, and *HST*, a total of 142 α Per and 100 Praesepe members with spectral types from B to early M and masses from ~5 to ~0.5 $M_\odot$ have been observed. Among the Praesepe sample is a total of 12 binaries, while there are 21 binaries and one triple in the larger α Per sample. In α Per, an additional six binaries and one quadruple are possible multiples with substellar companions. These potential substellar companions, however, require follow-up confirmation and are not included in the analysis. The detected systems range in separation from $0\farcs053$ to $\sim 5\farcs0$, with the majority newly resolved; only seven of the 41 multiples are previously known systems.

Because of the youth of these cluster stars, it is possible to test for correlations between the presence of a companion and signatures of stellar activity such as X-ray emission and rapid rotation. The combination of the data on α Per and Praesepe early-type stars with previous speckle and spectroscopic data on the Hyades shows that the majority, 0.6 ± 0.2, of late B and A-type stars with X-ray detections have companions; a CSF of only 0.21 ± 0.06 is measured for the stars in this spectral range without X-ray detections. This high CSF among X-ray targets suggests that the unexpected X-ray emission from these stars originates from later-type companions, although the small sample of early-type stars limits the statistical significance of the difference between the early-type stars with and without X-ray detections.

The role of companions to solar-type α Per stars in the wide range of rotational velocities measured for the members of this youngest cluster is also explored. Different theories have suggested that binaries should be associated with either the slow or the rapid rotators, but the $\mathrm{CSF}_{26\text{–}581\ \mathrm{AU}}$ for the slow rotators is indistinguishable from that of the rapid rotators. With the inclusion of the separations below 26 AU and fainter systems, the distribution of v sin i values is, however, significantly different for the binaries with separations less than 60 AU compared with the wider systems; the median v sin i for the close binaries is 105 ± 69 km s^{-1}, compared with 11 ± 21 km s^{-1} for the wide binaries. This suggests that the closest binaries may disrupt the circumstellar disk to such an extent that it cannot provide a braking mechanism.

Over the projected separation 26 to 581 AU and magnitude-difference range $\Delta K < 4$ ($q \gtrsim 0.25$), both α Per and Praesepe have a $\mathrm{CSF}_{26\text{–}581\ \mathrm{AU}}$ of 0.10 ± 0.03. This value is consistent with the $\mathrm{CSF}_{26\text{–}581\ \mathrm{AU}}$ for the intermediate-aged Pleiades cluster and the solar-aged G dwarfs, but significantly lower than the $\mathrm{CSF}_{26\text{–}581\ \mathrm{AU}}$ for nearby T Tauri stars. With the similarity in the 26–581 AU multiplicity from ~90 Myr to 5 Gyr, there is no evidence for a systematic decline in CSF that occurs on timescales less than 10^7 to 10^8 yr. Given the similarity in CSF for the clusters, the α Per, Praesepe, and Pleiades 26–581 AU binaries are combined and then merged with the Hyades/Praesepe spectroscopic and Hyades speckle data sets in order to construct an overall cluster CSF versus separation distribution spanning the range -1.75 to 2.75 in log (sep. [AU]). This results in an estimate of the total cluster CSF for $\Delta K \leq 4.0$ ($q \gtrsim 0.25$) of 0.48 ± 0.05. The cluster distribution peaks at 5 AU, a significantly smaller value than the solar-neighborhood and nearby T Tauri star distribution peaks. Taking the cluster and T Tauri distributions as representative of their initial populations, a simple population synthesis model leads to the suggestion that the nearby G dwarf binary distribution is a combination of approximately one-third dark cloud T Tauri binaries and two-thirds cluster/GMC binaries.

The observational results from the combined cluster sample involving the CSF and q-distribution were compared with a number of binary formation scenarios. Considering all binaries with separations from 26 to 581 AU and with mass ratios from 0.40 to 1.0, the q-distribution rises slightly toward lower q. This result is consistent with disk-assisted small-N capture, but the slope is too shallow to be explained by random pairing from a Salpeter mass function and too steep to be consistent with diskless small-N capture. The mass and separation dependence of the CSF and q-distribution represent important tests of other simulations. A trend of increasing CSF with decreasing mass is seen over the range of the sample, and the q-distribution of systems with $M_{\rm prim} \gtrsim 1.2\ M_{\odot}$ (B–F stars) is significantly different from that of the systems with $M_{\rm prim} \lesssim 1.2\ M_{\odot}$ (G and later stars), with a steeper slope (fewer $q \sim 1$ systems) associated with the higher mass primaries. The later result is predicted by both dynamical decay of small groups of stars and accretion in clusters but contradicts accretion simulations in loose associations. The presence of a clear mass dependence in the q-distribution and a strong suggestion of one in the CSF is inconsistent with scale-free fragmentation. Finally, the overall q-distribution does not vary with separation, which may be difficult to explain with models of disk fragmentation. In summary, the observational results are consistent with disk-assisted small-N capture, dynamical decay of three- to five-body systems, random capture from a cluster mass function, and accretion following fragmentation in a cluster, and they contradict the predictions of several other formation scenarios—random capture from a Salpeter mass function, diskless small-N capture, disk fragmentation, scale-free fragmentation, and accretion following fragmentation in a loose environment.

J. P. and A. M. G. were Visiting Astronomers at the Infrared Telescope Facility, which is operated by the University of Hawaii under contract from the National Aeronautics and Space Administration. Some of the data presented in this paper were obtained at the W. M. Keck Observatory, which is operated as a scientific partnership among the California Institute of Technology, the University of California, and the National Aeronautics and Space Administration. The Observatory was made possible by the generous financial support of the W. M. Keck Foundation. The authors wish to extend special thanks to those of Hawai'ian ancestry on whose sacred mountain we are privileged to be guests. Without their generous hospitality, these observations would not have been possible. With great appreciation, we thank the many people who have helped obtain the large amount of data required for this project: Alycia Weinberger at Palomar; Russel White, Lisa Prato, and Angelle Tanner at the IRTF; Al Schultz for *HST*; and Caer McCabe at Keck. We thank the telescope operators for their assistance with our observing program: Juan Carrasco and Rick Burruss at Palomar; Bill Golisch, Dave Griep, and Charlie Kaminsky at the IRTF; and Barbara Schaeffer and Theresa Chelminiak at Keck. Finally, we thank the referee, Rainer Köhler, for his helpful suggestions. This work benefited from the Open Cluster Database, as provided by C. F. Prosser (deceased) and J. R. Stauffer.[4]. Support for this work was provided by grant NAG 5-6975 through the Origins of Solar Systems Project, grant GO-07833.01-96A from the Space Telescope Science Institute, and a Packard Foundation fellowship. J. P. also received support from a dissertation-year fellowship from the American Association of University Women. Some of this work was performed under the auspices of the US Department of Energy by the University of California, Lawrence Livermore National Laboratory, under contract W-7405-ENG-48. This research required extensive use of the SIMBAD database, operated at CDS, Strasbourg, France.

[4] May currently be accessed at http://cfa-www.harvard.edu/~stauffer/opencl or by anonymous ftp to cfa-ftp.harvard.edu, cd /pub/stauffer/clusters.

APPENDIX A

COMPARISON WITH PREVIOUS α PERSEI AND PRAESEPE SURVEYS

Both α Per and Praesepe have been targeted by a number of previous binary star searches employing a variety of techniques—spectroscopy, lunar occultation, optical speckle, and direct imaging. These surveys provide information about binaries with separations that complement the current IR speckle survey. Since many of these previous surveys include only a subset of the brighter stars, it is not currently possible to obtain a complete census of multiple systems.

A1. PRAESEPE

Praesepe has been surveyed by several techniques covering a wide range of separations. Spectroscopic studies of the early-type stars and photometric binaries have detected the closest binaries in the cluster. A survey of Praesepe A stars (Burkhart & Coupry 1998) includes nine stars in the IR speckle sample. Notes in Tables 5 and 7 indicate the three singles and six binaries—KW 40, 224, 276, 279, 300, and 350—detected by this radial velocity survey. One of the spectroscopic binaries—KW 224—also has a $\sim$1″ speckle pair, making it a triple system; the other spectroscopic binaries are speckle singles. Another spectroscopic survey targeting stars located above the main sequence in the Hertzsprung-Russell diagram includes eight stars from this sample; five are spectroscopic singles and three are spectroscopic multiples—KW 365, 292, and 142 (Bolte 1991). One of the spectroscopic binaries—KW 365—is also a speckle binary; this speckle companion may explain why KW 365 is an SB3 system (Mermilliod, Duquennoy, & Mayor 1994), and it is counted as a triple rather than a quadruple. Results from long-term radial velocity monitoring surveys of Praesepe (Mermilliod & Mayor 1999; Abt & Willmarth 1999) include 49 of the 98 members (two of 100 targets are nonmembers) observed in the IR sample—41 speckle singles and eight speckle binaries. Notes about the individual stars are included in Tables 5 and 7. Of the 41 speckle singles, one is a triple—KW 40—and 16 are spectroscopic binaries—KW 534, 16, 47, 50, 142, 181, 182, 229, 268, 279, 300, 341, 371, 416, 479, and 496. Among the eight speckle binaries monitored spectroscopically, four are either spectroscopic systems with long periods or photometric/visual systems that suggest that they are binary, not triple, stars—KW 284, 275, 458, and 224. One of the speckle binaries is also a spectroscopic system, but with a short period that indicates it is a triple star—KW 365.

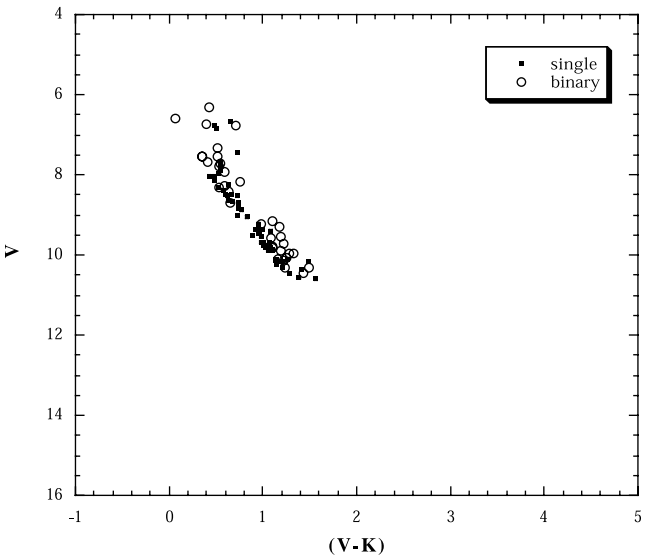

FIG. 11.—Praesepe sample color-magnitude diagram. The (V, $V-K$) color-magnitude diagram is plotted for the observed Praesepe stars excluding the stars determined to be nonmembers and the three G and K giants in the sample that were saturated in 2MASS photometry. Single stars are labeled with filled squares, while binary stars are denoted with open circles and account for most of the stars above the main sequence. These stars have been well surveyed by multiple techniques, and the binaries detected by any method are included in the figure. A detailed listing of the binaries is given in Tables 5 and 7.

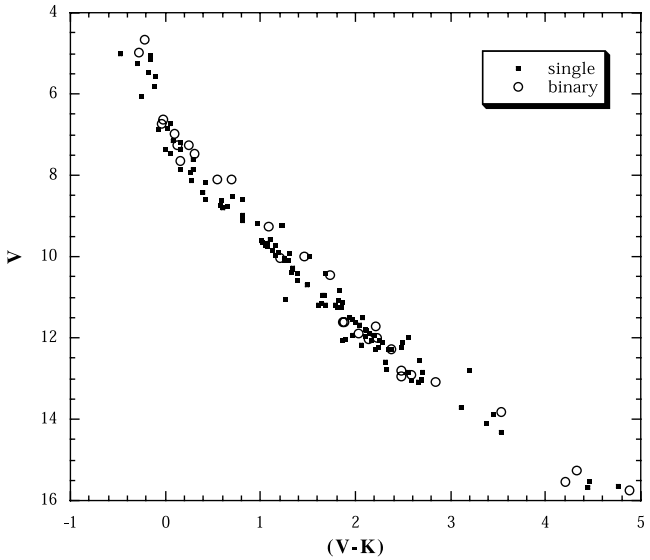

FIG. 12.—The α Per sample color-magnitude diagram. The (V, $V-K$) color magnitude diagram is plotted for all stars in the observed α Per sample. Single stars are marked with a filled square, and any known binary stars are distinguished by open circles. The faint potential substellar companions in the *HST* data set are not included, as those systems require additional confirmation. The α Per cluster has not been as comprehensively searched for binaries as Praesepe, however, and a significant number of multiple systems are probably not yet identified. The binaries included in this plot are listed in Tables 4A and 6.

Lunar occultation measurements detect the next closest set of binaries. Peterson & White (1984) observed 27 stars of this Praesepe sample and resolved three of them—KW 212, 143, and 203. Both KW 212 and KW 203 are detected by the IR survey, but KW 143 has a separation below the limit of the IR speckle survey. An optical speckle survey by Mason et al. (1993) has 48 stars in common with this IR study, and four of these 48 stars are resolved—KW 265, 284, 212, and 203. Three binaries—KW 212, 203, and 284—are also detected by IR speckle, but the companion to KW 265 is not seen in either Palomar speckle or IRTF shift-and-add observations, despite the relatively wide separation of 0.″425 measured by optical speckle. An additional three of the 48 stars—KW 385, 224, and 232—are binaries based on this IR survey, but not by the optical speckle measurements. KW 385 is outside the optical speckle field of view, and the remaining two systems have ΔK-values that correspond to ΔV-values fainter than the optical speckle $\Delta V = 3$ detection limit (Mason et al. 1993). An additional 15 visual binaries are compiled in the ADS, IDS, and WDS catalogs (Aitken 1932; Jeffers & van den Bos 1963; Mason et al. 2001), and the projected separations range from 1.″4 to 99.″68. The two systems with separations less than 3.″4 (the IRTF camera field of view)—KW 224 and KW 385—are both resolved by the IR speckle measurements. The remaining 13 systems are not considered physically associated, since even the closest pair has a separation as large as $\sim$21.″ Excluding the 13 widest pairs results in a lower limit to the overall single : binar-binary : triple : quadruple ratio of 67 : 28 : 3 : 0 and a total CSF of 0.38 ± 0.06 for the observed Praesepe speckle sample. Figure 11 plots a color-magnitude diagram for the Praesepe sample with the binaries detected by any technique indicated.

A2. α PERSEI

Although α Per has not been as extensively surveyed as Praesepe, a number of spectroscopic and visual binaries are known in the cluster. In a spectroscopic survey of early spectral type members, Morrell & Abt (1992) observed 23 stars in this IR sample and discovered four binaries among them—HE 423, 817, 774, and 775. An additional three systems—HE 868, 955, and 965—are categorized as probable SB1 stars (Morrell & Abt 1992). Because HE 965 also has a speckle companion, this system is a triple. Another two spectroscopic binaries in the speckle sample—HE 848 and HE 143—are reported by J.-C. Mermilliod (1991, private communication cited in Prosser 1992). Membership surveys also detect spectroscopic binaries, and one system—HE 314—is listed as a binary, while another system—HE 285—is listed as a probable spectroscopic binary by Prosser (1992). The HE 285 system is also resolved by speckle, and it is counted as a binary rather than a triple.

A total of eight visual binaries are listed in α Per (Aitken 1932; Jeffers & van den Bos 1963), with separations ranging from 0.″68 to 26.″91. HE 835 and HE 1082 have separations within the IRTF camera field of view. The visual binary HE 835 is also seen in the IR data, but HE 1082 was not detected by this survey; HE 1082 has a reported separation of 2.″05 in 1881 (Aitken 1932), but no subsequent measurements. The remaining six of these systems—HE 665, HD 18537/18538, and HE 955, 490, 799, and 828—have projected separations greater than 3.″4. The closest five of these six visual binaries are considered physically associated, since the probability that these systems are chance projections is less than 50% (based on the same estimation as in § 4.1). The widest system—HE 955—is not counted as a binary, because the probability that it is a background object exceeds 50% and

successive measurements show that the two stars do not share a common proper motion. This accounting results in a lower limit single : binary : triple : quadruple ratio of 112 : 28 : 3 : 0 and a CSF of 0.24 ± 0.04 for the α Per sample. Figure 12 plots a color-magnitude diagram for the α Per sample with the binaries detected by any technique indicated.

APPENDIX B

MAGNITUDES AND MASSES

The ground-based data for α Per and Praesepe only measure ΔK for the binaries and $\Delta K_{\rm lim}$ for the singles, but absolute M_K magnitudes for each star are needed to determine mass ratios and mass ratio limits. The single-star or binary system K magnitudes, the stellar distances, and the extinction are required to convert the ΔK and $\Delta K_{\rm lim}$ into binary $M_{K,1}$ and $M_{K,2}$ and single M_K and $M_{K,\rm lim}$, from which masses are determined with mass-magnitude relations. The K-band mass-magnitude relations are taken from Henry & McCarthy (1993) for the solar-mass and lower targets, and an extension to higher mass stars listed in Patience et al. (1998) is used for the early-type stars. The relations are repeated here:

$$\log\frac{M}{M_\odot} = \begin{cases} -0.159M_K + 0.49\ , & \text{for } M_K < 3.07\ , \\ -0.1048M_K + 0.3217\ , & \text{for } M_K = 3.07\text{–}5.94\ , \\ -0.2521M_K + 1.1965\ , & \text{for } M_K = 5.94\text{–}7.70\ , \\ -0.1668M_K + 0.5395\ , & \text{for } M_K = 7.70\text{–}9.81\ . \end{cases}$$

For the majority of the cluster stars, K_s measurements are available from the 2MASS database (Cutri et al. 2001). Since the mass-magnitude relations are based on K rather than K_s, the 2MASS K_s-values are converted to K-values based on the transformation

$$K = K_{\rm CIT} = (K_s)_{\rm 2MASS} + 0.024\ ,$$

given in Carpenter (2001). The Caltech (CIT) system is chosen because it is closest to that used in the photometry for constructing the mass-magnitude relations.

The current 2MASS data release covers the majority of the sources considered in this work. Of the 544 sources considered in this work, only 26 α Per targets, 13 Praesepe targets, seven Pleiades binaries, and seven Hyades binaries are not included in the 2MASS point-source catalog. For the α Per and Praesepe samples, the stars measured by 2MASS are used to construct a V-$(K_s)_{\rm 2MASS}$ relation from which the K for each star without a 2MASS measurement is estimated. The empirical V-$(K_s)_{\rm 2MASS}$ fit is

$$(K_s)_{\rm 2MASS} = -3.34 + 12.14\log V$$

for α Per and

$$(K_s)_{\rm 2MASS} = -5.69 + 14.49\log V$$

for Praesepe. System K magnitudes for the Pleiades binaries not in the 2MASS sample are taken from measurements given in Bouvier et al. (1997). For the Hyades binaries not covered by 2MASS, the system K magnitude is estimated by converting the $B-V$ color into a $V-K$ color based on the relation given in Patience et al. (1998). These alternate methods, which affect only a small portion of the sample, were checked for stars with 2MASS measurements and yield magnitudes within 10% of the 2MASS values. Once the absolute system magnitude is determined by

$$M_{K,\rm system} = K_{\rm system} - 5\log(D/10) - A_K\ ,$$

the primary and secondary absolute magnitudes are given by

$$\begin{aligned} M_{K,\rm prim} &= M_{K,\rm system} + 2.5\log(1 + 10^{-\Delta K/2.5})\ , \\ M_{K,\rm sec} &= M_{K,\rm prim} + \Delta K\ , \end{aligned}$$

and these values are substituted into the appropriate mass-magnitude relation. The distances to α Per, Praesepe, and the Pleiades are taken from Pinsonneault et al. (1998) and are given in §§ 2 and 4.3.1. The distances to the Hyades members are determined individually by scaling values from Schwan (1991) or Reid (1992), as described in Patience et al. (1998). There is no reddening correction for Praesepe or the Hyades, but A_K is 0.035 for α Per and 0.014 for the Pleiades based on the $E(B-V)$ listed in Pinsonneault et al. (1998) and the relations given by Rieke & Lebofsky (1985).

For the α Per stars observed with *HST*, a similar procedure was used with J magnitudes instead of K. In this case, the data provide ΔF140W and ΔF140W$_{\rm lim}$, so an extra step of changing the F140W into J is required. The single stars with measured 2MASS J magnitudes were converted to $J_{\rm CIT}$ with the relation from Carpenter (2001),

$$J_{\rm CIT} = 0.947J_{\rm 2MASS} + 0.053K_{\rm 2MASS} + 0.36\ .$$

As with the K-band data, the four stars that were not observed with 2MASS were assigned estimated $J_{\rm 2MASS}$ magnitudes based on their V magnitudes with the relation

$$J_{\rm 2MASS} = -5.72 + 14.8\log V\ .$$

After switching the measured or estimated 2MASS magnitudes to the CIT system, the single stars were used to construct an F140W-J relation (the zero point is arbitrary):

$$J_{\rm CIT} = -3.42 + 1.03(\text{F140W})\ .$$

Since the slope is not exactly unity, the observed ΔF140W values are multiplied by the slope 1.03 to obtain ΔJ. The extinction A_J for α Per is 0.087. With the absolute M_J system determined, the component absolute magnitudes are solved for, and the masses are estimated with the Henry & McCarthy (1993) relations

$$\log\frac{M}{M_\odot} = \begin{cases} -0.0863M_J + 0.3007\ , & \text{for } M_J = 3.48\text{–}6.97\ , \\ -0.2791M_J + 1.6440\ , & \text{for } M_J = 6.97\text{–}8.56\ , \\ -0.1593M_J + 0.6177\ , & \text{for } M_J = 8.56\text{–}10.77\ . \end{cases}$$

APPENDIX C

CSF DISTRIBUTION DETAILS

The tables and explanations in this appendix are designed to help reconstruct the CSF distributions of open cluster stars, field G dwarfs, nearby T Tauri stars, and T Tauri stars in Orion that are plotted in Figures 4*a*–4*d*. Tables A1–A3

TABLE A1

CLUSTER BINARIES IN FIGURE 3*a*

log (sep. [AU])	Sample Size	No. Bin	Clusters	Techniques	Refs.	Binaries
−1.525	162	3	Hyades	Spectroscopy	1	Lei 20; BD +22°669; vB 38
−1.075	241	9	Hyades, Praesepe	Spectroscopy	1, 2	vB 34, 40, 22, 121, 45, 62, 117; KW 181, 127
−0.625	262	14	Hyades, Praesepe	Spectroscopy	1, 2, 3	vB 112, 75, 69, 162; Lei 83; KW 416, 47, 495, 142, 184, 365, 368, 300, 284
−0.175	262	11	Hyades, Praesepe	Spectroscopy	1, 2, 3	vB 83, 124, 130, 140, 77, 185, 182; KW 268, 534, 428, 40
0.275	241	15	Hyades, Praesepe	Spectroscopy	1, 2	vB 177, 95, 43, 102, 151; Lei 63; BD +10°568; vB 142, 115, 120; KW 439, 508, 325, 540, 367
0.725	162	18	Hyades	Spectroscopy, speckle	1, 4	Lei 57, 90; vB 57, 63, 96, 113, 81, 106, 91, 39; Lei 59; vB 141, 24, 103, 114, 50, 59, 58
1.175	162	11	Hyades	Speckle	1, 4	Lei 20, 83; vB 102, 131, 85, 122, 75; Lei 92; vB 29, 185, 124
1.625	383	15	α Per, Pleiades, Praesepe	Speckle, AO, shift-and-add	5, 6	KW 275; HE 285; HII 2106, 1061; A 1565; KW 232, 458; HII 2278; AP 149AB; KW 365; HII 738, 357, 2500AC; AP 139, 98
2.075	383	16	α Per, Pleiades, Praesepe	Speckle, AO, shift-and-add	5, 6	AP 38; HII 3197AC; KW 203; HII 2193; AP 201, 41; HII 97, 1100, 885; HE 835; KW 250; HII 1298; KW 224; HII 1355; AP 17; KW 282
2.525	383	9	α Per, Pleiades, Praesepe	Speckle, AO, shift-and-add	5, 6	MT 61AB; HII 303, 134; HE 780AC, 828; KW 385; AP 6; HII 102; AP 121

REFERENCES.—(1) Griffin et al. 1988; (2) Mermilliod & Mayor 1999; (3) Abt & Willmarth 1999; (4) Patience et al. 1998; (5) Bouvier et al. 1997; (6) this work.

TABLE A2

T Tauri Binaries in Figure 3*c*

log (sep. [AU])	Sample Size	No. Bin	Regions	Techniques	Refs.	Binaries
−1.525	53	1	Tau/CrA/Sco-Oph	Spectroscopy	1	NTTS 155913−2233
−1.075	53	1	Tau/CrA/Sco-Oph	Spectroscopy	1	NTTS 160905−1859
−0.625	53	2	Tau/CrA/Sco-Oph	Spectroscopy	1	NTTS 162819−2423S, 162814−2427
−0.175	53	1	Tau/CrA/Sco-Oph	Spectroscopy	1	NTTS 160814−1857
0.275	82	5	Tau/Oph	Lunar occultation	2	V853 Oph; ROXs 43B; HP Tau; SR 1; HP Tau G3/G2
0.725	82	5	Tau/Oph	Lunar occultation	2	Elias 12; FF Tau; ZZ Tau; HV Tau; ROXs 42B
1.175	101	10	Tau/Oph	Lunar occultation, speckle	2, 3	SR 20; DF Tau; VSSG 14; FW Tau; ROX 42C; V773 Tau; DI Tau; V410 Tau; V928 Tau; FO Tau
1.625	254	29	Tau/Tau (X)/Lup/ Cha/CrA	Speckle	2, 3, 4, 5, 6	SR 12; ROXs 31; GN Tau; V853 Oph; LkCa 3; IW Tau; LkHα 331; CoKu LkHα 332/G2; GH Tau; XZ Tau; CZ Tau; Elias 12; CoKu LkHα 332/G1; GG Tau; LkHα 332; IS Tau; FS Tau; HN Lup; HM Anon; RX J0444.4 + 1952AB, RX J0438.2 + 2023, RX J0452.8 + 1621; HD 284135; RX J0451.9 + 2849 B; RX J0420.8 + 3009AB; UZ Tau W; RX J0452.9 + 1920; BD + 26°718B-Aa; Haro 6-37AC
2.075	254	26	Tau/Tau (X)/Lup/ Cha/CrA	Speckle, direct imaging	3, 4, 5, 6	NTTS 043230 + 1746; FQ Tau; Haro 6-28; DD Tau; FX Tau; UY Aur; VY Tau; NTTS 034903 + 2431; T Tau; C 7-11; S CrA; VW Cha; WX Cha; RX J0457.2 + 1524, RX J0447.9 + 2755; FV Tau, FV Tau/c; RX J0451.8 + 1758, RX J0453.1 + 3311AB; LkCa 7; HD 285281; RX J0415.8 + 3100; RW Aur A/B; GG Tau; RX J0415.3 + 2044; Haro 6-10
2.525	254	19	Tau/Tau (X)/Lup/ Cha/CrA	Direct imaging	2, 4, 5, 6	Sz 41; NTTS 040047 + 2603; RX J0444.9 + 2717; Sz 77, 81; DoAr 24 E; CoKu Tau 3; VV CrA; IT Tau; CHXR 32; RX J0412.8 + 1937; Haro 6-37/c; UX Tau A/B; Sz 120; VW Cha; DK Tau; Sz 68; V710A/B, UZ Tau E/W
2.975	240	19	Tau/Tau (X)/Lup/ Cha/CrA	Direct imaging	4, 5, 6	Sz 65, 91; RX J0437.4 + 185, RXJ0444.4 + 1952AB-C, RX J0420.8 + 3009AB-C, RX J0409.1 + 2901, RX J0457.5 + 2014, RX J0453.1 + 3311AB-C; BD + 26°718B; RX J0438.2 + 2302; HD 285957AB; RX J0444.3 + 2017, RX J0431.3 + 1800, RX J0435.9 + 2352AB-C; UX Tau A/B; NTTS 040142 + 2150 W + E, NTTS 035120 + 3154; GG Tau; HP Tau

References.—(1) Mathieu et al. 1989; (2) Simon et al. 1995; (3) Ghez et al. 1993; (4) Leinert et al. 1993; (5) Köhler & Leinert 1998; (6) Ghez et al. 1997.

TABLE A3
ORION BINARIES IN FIGURE 3*c*

log (sep. [AU])	Sample Size	No. Bin	Techniques	Refs.	Binaries
−1.525	...	...	...		
−1.075	...	...	...		
−0.625	...	...	...		
−0.175	...	...	...		
0.275	...	...	...		
0.725	...	...	...		
1.175	...	...	...		
1.625	361	11	*HST* imaging, speckle	1, 2	TCC 56; PC 11/12, 13/14, 80/79, 99/98, 126/125, 152/150, 173/172, 202/203, 208/206, 322/321
2.075	480	20	*HST* imaging, speckle, AO	1, 2, 3	TCC 45, 77/75, 101; PC 16/17, 33/34, 48/49, 68/67, 111/112, 144/143, 224/222, 315/314; AO 45/46, 102/104, 128/131, 5/6, 16/18, 29/30, 149/147, 179/180, 183/185
2.525	480	16	*HST* imaging, speckle, AO	1, 2, 3	PC 37/40, 57/58, 80/77, 129/130, 219/221, 235/234, 282/279, 294/296, 323/324; AO 51/48, 74/78, 110/116, 117/110, 117/116, 184/189, 253/252

REFERENCES.—(1) Prosser et al. 1994; (2) Petr et al. 1998; (3) Simon et al. 1999.

list the binaries included in each separation bin and give references for the surveys from which the binaries were drawn. Whenever possible, the binaries counted from each survey are limited to the binaries with separations in which the entire bin is covered by the survey. The one exception to this is the log (sep. [AU]) = 0.95–1.4 bin in the nearby T Tauri distribution; the closest speckle systems resolved with the 5 m Hale are included, although this data set is not as sensitive to all separations covered by this bin. For the open clusters and the nearest star-forming regions, some additional binaries are known but not included. Some binaries exceed the $\Delta K = 4$ mag limit, and others have separations placing them in bins not entirely covered by the survey.

Because the original G dwarf distribution (Duquennoy & Mayor 1991) includes corrections, it is not possible to generate an analogous table indicating which binaries are included in the individual bins. Instead, the distribution shown in Figures 4*b* and 5 is a scaled version of the original Figure 7 plot in Duquennoy & Mayor (1991). Two scalings are required: one reduction to account for the sensitivity difference and a second decrease in the number of companions due to the smaller bin size of the distributions in Figure 4*a*–4*d*. The log (sep.) bins are two-thirds the width of the G dwarf log (*P* [days]) bins, so Figure 4*b* incorporates the bin size scaling and Figure 5 includes the additional sensitivity scaling. For example, the log (sep.) = 0.95–1.4 bin is 67% of the $\Delta \log P = 4$–5 bin, which includes 18 companions including corrections in the original G dwarf distribution; the corresponding number of companions in Figure 4*b* is 12, or a CSF of 0.074. In Figure 5, the G dwarf curve is further scaled down by 16%, as discussed in § 4.3.3, to account for the difference in sensitivity.

REFERENCES

Aarseth, S. J., & Hills, J. G. 1972, A&A, 21, 255
Abt, H. A. 1965, ApJS, 11, 429
Abt, H. A., & Levy, S. G. 1976, ApJS, 30, 273
Abt, H. A., & Willmarth, D. W. 1999, ApJ, 521, 682
Adams, F. C., & Myers, P. C. 2001, ApJ, 553, 744
Aitken, R. G. 1932, New General Catalogue of Double Stars within 120° of the North Pole (Carnegie Inst. Washington Publ. 417) (Washington: Carnegie Inst.)
Armitage, P. J., & Clarke, C. J. 1996, MNRAS, 280, 458
Baraffe, I., Chabrier, G., Allard, F., & Hauschildt, P. H. 1998, A&A, 337, 403
Bate, M. R. 2000, MNRAS, 314, 33
———. 2001, in IAU Symp. 200, The Formation of Binary Stars, ed. H. Zinnecker & R. D. Mathieu (San Francisco: ASP), 429
Bate, M. R., & Bonnell, I. A. 1997, MNRAS, 285, 33
Bates, R. H. T., & Cady, F. M. 1980, Opt. Commun., 32, 365
Bertout, C. 1989, ARA&A, 27, 351
Bolte, M. 1991, ApJ, 376, 514
Bonnell, I. A., & Bate, M. R. 1994, MNRAS, 271, 999
Boss, A. P. 1996, ApJ, 468, 231
Bouvier, J., & Corporon, P. 2001, in IAU Symp. 200, The Formation of Binary Stars, ed. H. Zinnecker & R. D. Mathieu (San Francisco: ASP), 155
Bouvier, J., Rigaut, F., & Nadeau, D. 1997, A&A, 323, 139
Brandner, W., & Köhler, R. 1998, ApJ, 499, L79
Burkhart, C., & Coupry, M. F. 1989, A&A, 220, 197
———. 1998, A&A, 338, 1073
Carpenter, J. M. 2001, AJ, 121, 2851
Christou, J. C. 1991, PASP, 103, 1040
Clarke, C. 1996a, in Evolutionary Processes in Binary Stars, ed. R. A. M. J. Wijers, M. B. Davies, & C. A. Tout (NATO ASI Ser. C, 477) (Dordrecht: Kluwer), 31
Clarke, C. J. 1996b, MNRAS, 283, 353
Cutri, R. M., et al. 2001, Explanatory Supplement to the 2MASS Second Incremental Data Release (Pasadena: Caltech)
Duquennoy, A., & Mayor, M. 1991, A&A, 248, 485
Durisen, R. H., & Sterzik, M. F. 1994, A&A, 286, 84
Fischer, D. A., & Marcy, G. W. 1992, ApJ, 396, 178
Genzel, R., & Stutzki, J. 1989, ARA&A, 27, 41
Ghez, A. M., Klein, B. L., Morris, M., & Becklin, E. E. 1998, ApJ, 509, 678
Ghez, A. M., McCarthy, D. W., Patience, J. L., & Beck, T. L. 1997a, ApJ, 481, 378
Ghez, A. M., Neugebauer, G., & Matthews, K. 1993, AJ, 106, 2005
Ghez, A. M., White, R. J., & Simon, M. 1997b, ApJ, 490, 353
Gómez, M., Hartmann, L., Kenyon, S. J., & Hewett, R. 1993, AJ, 105, 1927
Griffin, R. F., Gunn, J. E., Zimmerman, B. A., & Griffin, R. E. M. 1988, AJ, 96, 172
Hartigan, P., Strom, K. M., & Strom, S. E. 1994, ApJ, 427, 961
Heckmann, O., Dieckvoss, W., & Kox, H. 1956, Astron. Nachr., 283, 109
Henry, T. J. & McCarthy, D. W., Jr. 1993, AJ, 106, 773
Herbst, W., Rhode, K. L., Hillenbrand, L. A., & Curran, G. 2000, AJ, 119, 261
Jeffers, H. M. & van den Bos, W. H. M. 1963, Index Catalogue of Visual Double Stars, 1961.0 (Publ. Lick Obs. 21) (Mt. Hamilton, CA: Lick Obs.)
Jensen, E. L. N., Mathieu, R. D., & Fuller, G. A. 1994, ApJ, 429, L29
———. 1996, ApJ, 458, 312
Kenyon, S. J., & Hartmann, L. 1995, ApJS, 101, 117
Klein Wassink, W. J. 1927, Publ. Kapteyn Astron. Lab. Groningen, No. 41
Köhler, R. & Leinert, C. 1998, A&A, 331, 977
Königl, A. 1991, ApJ, 370, L39
Kroupa, P. 1995a, MNRAS, 277, 1491
———. 1995b, MNRAS, 277, 1522

Labeyrie, A. 1970, A&A, 6, 85
Lada, E. A., Evans, N. J., II, DePoy, D. L., & Gatley, I. 1991, ApJ, 371, 171
Leinert, C., Zinnecker, H., Weitzel, N., Christou, J., Ridgway, S. T., Jameson, R., Haas, M., & Lenzen, R. 1993, A&A, 278, 129
Lohmann, A. W., Weigelt, G., & Wirnitzer, B. 1983, Appl. Opt., 22, 4028
Macintosh, B., Zuckerman, B., Becklin, E. E., & McLean, I. S. 2000, ApJ, submitted
Mason, B. D., Hartkopf, W. I., McAlister, H. A., & Sowell, J. R. 1993, AJ, 106, 637
Mason, B. D., Henry, T. J., Hartkopf, W. I., ten Brummelaar, T., & Soderblom, D. R. 1998, AJ, 116, 2975
Mason, B. D., Wycoff, G. L., Hartkopf, W. I., Douglass, G. G., & Worley, C. E. 2001, AJ, 122, 3466
Mathieu, R. D., Walter, F. M., & Myers, P. C. 1989, AJ, 98, 987
Matthews, K., Ghez, A. M., Weinberger, A. J., & Neugebauer, G. 1996, PASP, 108, 615
Matthews, K., & Soifer, B. T. 1994, in Infrared Astronomy with Arrays: The Next Generation, ed. I. S. McLean (Dordrecht: Kluwer), 239
Mazeh, T., Goldberg, D., Duquennoy, A., & Mayor, M. 1992, ApJ, 401, 265
McCaughrean, M. J., & Stauffer, J. R. 1994, AJ, 108, 1382
McDonald, J. M., & Clarke, C. J. 1993, MNRAS, 262, 800
———. 1995, MNRAS, 275, 671
Mermilliod, J.-C. 1981, A&A, 97, 235
Mermilliod, J.-C., Duquennoy, A., & Mayor, M. 1994, A&A, 283, 515
Mermilliod, J.-C., & Mayor, M. 1999, A&A, 352, 479
Meusinger, H., Schilbach, E., & Souchay, J. 1996, A&A, 312, 833
Miller, G. E., & Scalo, J. M. 1978, PASP, 90, 506
Morrell, N., & Abt, H. A. 1992, ApJ, 393, 666
Oppenheimer, B. R. 1999, Ph.D. thesis, Caltech
Osterloh, M., & Beckwith, S. V. W. 1995, ApJ, 439, 288
Pallavicini, R. 1989, A&A Rev., 1, 177
Patience, J., Ghez, A. M., Reid, I. N., Weinberger, A. J., & Matthews, K. 1998, AJ, 115, 1972
Perryman, M. A. C., et al. 1998, A&A, 331, 81
Peterson, D. M., & White, N. M. 1984, AJ, 89, 824
Petr, M. G., Coudé du Foresto, V., Beckwith, S. V. W., Richichi, A., & McCaughrean, M. J. 1998, ApJ, 500, 825
Pinsonneault, M. H., Stauffer, J., Soderblom, D. R., King, J. R., & Hanson, R. B. 1998, ApJ, 504, 170
Prosser, C. F. 1992, AJ, 103, 488
Prosser, C. F., Randich, S., Stauffer, J. R., Schmitt, J. H. M. M., & Simon, T. 1996, AJ, 112, 1570
Prosser, C. F., Stauffer, J. R., Hartmann, L., Soderblom, D. R., Jones, B. F., Werner, M. W., & McCaughrean, M. J. 1994, ApJ, 421, 517
Randich, S., & Schmitt, J. H. M. M. 1995, A&A, 298, 115 (erratum 303, 322)
Randich, S., Schmitt, J. H. M. M., Prosser, C. F., & Stauffer, J. R. 1996, A&A, 305, 785
Rayner, J. T., et al. 1993, Proc. SPIE, 1946, 490
Reid, I. N., & Gizis, J. E. 1997, AJ, 114, 1992
Reid, I. N., Gizis, J. E., Kirkpatrick, J. D., & Koerner, D. W. 2001, AJ, 121, 489
Reid, N. 1992, MNRAS, 257, 257
Rieke, G. H., & Lebofsky, M. J. 1985, ApJ, 288, 618
Scally, A., Clarke, C., & McCaughrean, M. J. 1999, MNRAS, 306, 253
Schatzman, E. 1962, Ann. d'Astrophys., 25, 18
Schwan, H. 1991, A&A, 243, 386
Shure, M. A., Toomey, D. W., Rayner, J. T., Onaka, P. M., & Denault, A. J. 1994, Proc. SPIE, 2198, 614
Simon, M., Close, L. M., & Beck, T. L. 1999, AJ, 117, 1375
Simon, M., Ghez, A. M., & Leinert, C. 1993, ApJ, 408, L33
Simon, M., et al. 1995, ApJ, 443, 625
Stassun, K. G., Mathieu, R. D., Mazeh, T., & Vrba, F. J. 1999, AJ, 117, 2941
Stauffer, J. R., et al. 1999, ApJ, 527, 219
Stauffer, J. R., Hartmann, L. W., Burnham, J. N., & Jones, B. F. 1985, ApJ, 289, 247
Stauffer, J. R., Schultz, G., & Kirkpatrick, J. D. 1998, ApJ, 499, L199
Stefanik, R. P., & Latham, D. W. 1992, in IAU Colloq. 135, Complementary Approaches to Double and Multiple Star Research, ed. H. A. McAlister & W. I. Hartkopf (ASP Conf. Ser. 32) (Chelsea, MI: ASP), 173
Stern, R. A., Schmitt, J. H. M. M., & Kahabka, P. T. 1995, ApJ, 448, 683
Sterzik, M. F., & Durisen, R. H. 1998, A&A, 339, 95
Thompson, R. I., Rieke, M., Schneider, G., Hines, D. C., & Corbin, M. R. 1998, ApJ, 492, L95
Torres, G., Stefanik, R. P., & Latham, D. W. 1997, ApJ, 474, 256
Tout, C. A., & Pringle, J. E. 1995, MNRAS, 272, 528
Udry, S., Mayor, M., Delfosse, X., Forveille, T., & Perrier-Bellet, C. 2000, in Poster Proc. IAU Symp. 200, Birth and Evolution of Binary Stars, ed. B. Reipurth & H. Zinnecker (Potsdam: Astrophys. Inst. Potsdam), 158
White, R. J. 1999, Ph.D. thesis, UCLA
White, R. J., & Ghez, A. M. 2001, ApJ, 556, 265
White, R. J., Ghez, A. M., Reid, I. N., & Schultz, G. 1999, ApJ, 520, 811
Zinnecker, H., & Preibisch, T. 1994, A&A, 292, 152